12-2022

Conjunctive Management for Groundwater-Surface Water Resources: Numerical Modeling and Potential Assessment of Managed Aquifer Recharge (MAR) at Lower Rio Grande Valley in South Texas

Dwight Zedric Q. Capus
The University of Texas Rio Grande Valley

CONJUNCTIVE MANAGEMENT FOR GROUNDWATER-SURFACE WATER RESOURCES: NUMERICAL MODELING AND POTENTIAL ASSESSMENT OF MANAGED AQUIFER RECHARGE (MAR) AT LOWER RIO GRANDE VALLEY IN SOUTH TEXAS

A Thesis

by

DWIGHT ZEDRIC Q. CAPUS

Submitted in Partial Fulfillment of the

Requirements for the Degree of

MASTER OF SCIENCE

Major Subject: Ocean, Coastal, and Earth Science

The University of Texas Rio Grande Valley

December 2022

CONJUNCTIVE MANAGEMENT FOR GROUNDWATER-SURFACE WATER RESOURCES: NUMERICAL MODELING AND POTENTIAL ASSESSMENT OF MANAGED AQUIFER RECHARGE (MAR) AT LOWER RIO GRANDE VALLEY IN SOUTH TEXAS

A Thesis
by
DWIGHT ZEDRIC Q. CAPUS

COMMITTEE MEMBERS

Dr. Chu-Lin Cheng
Chair of Committee

Dr. Jude Benavides
Committee Member

Dr. Abdoul Oubeidillah
Committee Member

December 2022

ABSTRACT

Capus, Dwight Zedric Q., Conjunctive Management for Groundwater-Surface Water Resources: Numerical Modeling and Potential Assessment of Managed Aquifer Recharge (MAR) at Lower Rio Grande Valley in South Texas. Master of Science (MS), December 2022, 74 pp., 15 tables, 45 figures, references 42 titles.

Texas is well known to frequent floods and droughts, and yet has mounting concerns in very imbalanced water availability and water demands from growth in population and economical activities. Capturing and storing water is essential to long-term and climate-smart management of the "already-scarce" water resources. This study aimed to apply numerical modeling to evaluate potentials and impacts of Managed Aquifer Recharge (MAR) to regional groundwater systems in the Lower Rio Grande Valley. Using Visual MODFLOW Flex 3D package, different scenarios were simulated for groundwater flow patterns and storage capacities. Water injections tested ranged between 7.30×10^5 ft^3 to 3.65×10^9 ft^3, which were comparable to existing ASR capacities in Texas. This study examined flow patterns and water table changes at one selected MAR site with injected water volume equivalent to 3~5% of flood water from Hurricane Hanna (major flood event in LRGV). Giving current assumptions and limited scenarios ran, study results showed that MAR injections had minimal impacts to regional coastal aquifers. LRGV are suitable for MAR using treated water or when there is surplus water, i.e., water from flooding as alternative mitigations. More studies such as data and simulations are needed to better plan and build water resilience.

DEDICATION

This research is dedicated to my parents/family, who have sacrificed so much to raise me to become the man I am today. I am eternally grateful to all who have supported my endeavors and inspired me to pursue higher education. By taking all the life lessons, and experiences shared I strive to continue being a better person, professional, and scientist each day.

ACKNOWLEDGMENTS

I would like to express my deepest gratitude to my major advisor and the thesis committee chair, Dr. Chu-Lin Cheng, for all his help, guidance, and patience that he has given me over the past two years in graduate school and during COVID pandemic. I would like also to express my gratitude to the committee members, Dr. Jude A. Benavides and Dr. Abdoul Oubeidillah, who generously provided their expertise and knowledge. Additionally, this work would not have been possible without the assistantship support from the School of Earth, Environmental, and Marine Sciences (SEEMS).

I would also like to thank many SEEMS faculty and staff such as Dr. Diego Figueroa, and Ms. Lorena Longoria, Dr. Juan Gonzalez, Ms. Sarah Hardage, for the support and timely assistance in past two years.

I also like to acknowledge several TWDB staff members (Texas Water Development Board) for many kind assistances throughout this process. During conceptual model construction stage, Dr. Shirley Wade shared existing groundwater models and geodatabases for the lower Rio Grande valley. Dr. Jerry Shi also was helpful for analysis, interpretation, and confirming bias and discrepancies between TWDB reports.

Lastly, words cannot express my gratitude to my parents, siblings, relatives for supporting and believing in me. I would not be on this path without them.

TABLE OF CONTENTS

Page

LIST OF TABLES

LIST OF FIGURES

Page

CHAPTER I

INTRODUCTION

Increasing water demand, more frequent and longer droughts, the invasion of saline waters or other water quality challenges, are all contributing to water resource stress (LaHaye et al. 2021). In Saudi Arabia, 97% of water usage come from groundwater supplies and water levels are declining at a rate that groundwater reserves will soon be exhausted, probably within 20 to 50 years. In Beijing, China, about one-third of the wells have supposedly gone dry and groundwater levels have been dropping about 3 to 6 ft per year (Pyne, 1995). These are only two of the many warning signs of increasingly, water demand as global population continues to grow. It is imperative to manage the water resources wisely and efficiently if we are to sustain the water needs of a rising population. To fulfill local needs, even more stringent water management approaches have lately been introduced in a few regions. Pumped storage projects to meet peak power needs, deep injection wells to dispose of wastewater and form salinity intrusion barriers, desalination of brackish and seawater, reclaimed water irrigation systems, increasingly sophisticated treatment plants to treat water and wastewater to potable standards, and artificial recharge facilities to replenish aquifers are just a few examples (Pyne, 1995).

Managed aquifer recharge (MAR, or aquifer recharge, AR in some literatures) is the intentional recharge aquifers by means of injection wells or other infiltration; for later recovery or for environmental reasons (Shaw et al., 2020). Water is stored in an aquifer the same as how

water is stored in a surface reservoir or tank for future use. When the water demand is low, the excess water can be stored. When there is an increase in demand for water or decrease in precipitation, the stored water can be recovered (Lowry & Anderson, 2006). Located in an arid to semi-arid environment, Texas is in deficit for water balance and is susceptible to increasing droughts. Texas is well known for declining water levels like many western states in the US. The demands for water oftentimes are difficult to meet by conservation and conventional strategies, especially the expensive and controversial surface reservoirs (Pirnie et al, 2011). It is critical to sustainable manage water resources to capture and store extra water when it is available, e.g., floods during hurricane seasons. The cost-effectiveness and environmental challenges related to surface water reservoirs have led water professionals to research ASR (a type of MAR). Even though ASR has proven to be cost-effective and is an efficient method of storing water, Pirnie and colleagues (2011) indicated that Texas is behind with respect to implementation of ASR comparing to other states (Pirnie et al, 2011).

This warrants the need for more in-depth studies on potential aquifer storage and possible site conditions across the state. With the absence of artificial recharge, groundwater levels in Texas are depleting at an exponential rate within a short period of time (Pirnie et al., 2011). Replenishing aquifers that have been overused for many years can help improve water security in Texas. This can be achieved through implantation of ASR as a part of the water storage plan and to build community resiliency for water shortage (Pirnie et al., 2011), and informed decisions for policy makers and stakeholders for municipalities in the LRGV. In a recent Texas Water Development Board (TWDB) report, LRGV is rated as a high MAR (AR) suitability region considering many screening parameters (TWDB, 2020)

Objective

The main research question of this study is “can ASR systems be used to improve water security and mitigate flood hazards in the LRGV?” More specifically, “what volume of water can be injected into the target hydrogeologic units in LRGV and at what injection rates?” To examine and this question, four main tasks were developed, which were:

(i) construct a conceptual groundwater model using hydrogeologic data currently available,

(ii) build a numerical groundwater model for LRGV,

(iii) perform scenario simulations of combinations of MAR at selected locations,

(iv) examine water quantity and injection rates with flood events for feasibility.

The model will provide outputs for site suitability and possible water resource management options for the region.

CHAPTER II

LITERATURE REVIEW

Managed aquifer recovery

Managed aquifer recharge (MAR, or Aquifer Recharge, AR in some literatures) is the intentional recharge aquifers by means of injection wells or other infiltration; for later recovery or for environmental reasons (Shaw et al., 2020). In conjunction with demand management techniques, MAR can be used to recharge depleted aquifers and restore hydrologic balance while minimizing negative effects on the livelihoods of irrigated communities. Managed aquifer recharge acts in conjunction with concurrent use of surface waters and groundwater to preserve water supplies and accomplish groundwater and surface water management goals, such as the preservation of ecosystems (Figure 1) (Jakeman et al., 2016). Other usage of MAR is being successfully used in different purposes. Among these are: (1) Maintaining minimum flows and levels: MAR can be used to maintain minimum levels in lakes or minimum flows in streams and rivers; (2) Flood mitigation: utilizing stormwater for MAR could help prevent flooding; (3) Water reuse: MAR is being used more and more to control the reuse of treated wastewater, frequently for irrigation and drinking water (Dillon et al , 2022).

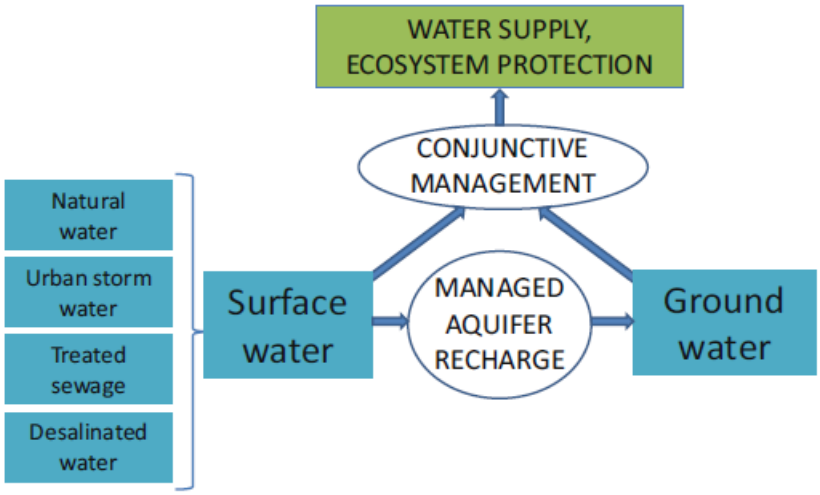

Figure 1. Roles of managed aquifer recharge (MAR) and conjunctive use in integrated water resources management (Dillon et al, 2022).

According to Dilon et al., (2022), there are different methods of MAR. Stream bed channel modifications, Bank infiltration, and Recharge wells (e.g., Aquifer Storage and Recovery (ASR), Aquifer Storage Transfer and Recovery (ASTR). Figure 2 shows various types of MAR. Figure 3 shows the schematic diagram of ASR which is a type of MAR. Aquifer storage and recovery (ASR) is a technological method of enhancing natural groundwater recharge through man-made infiltration basins or injection wells in order to reclaim the water at a later period. Without the recovery operation, the method is commonly referred to as aquifer recharge (AR) (Yang, 2016).

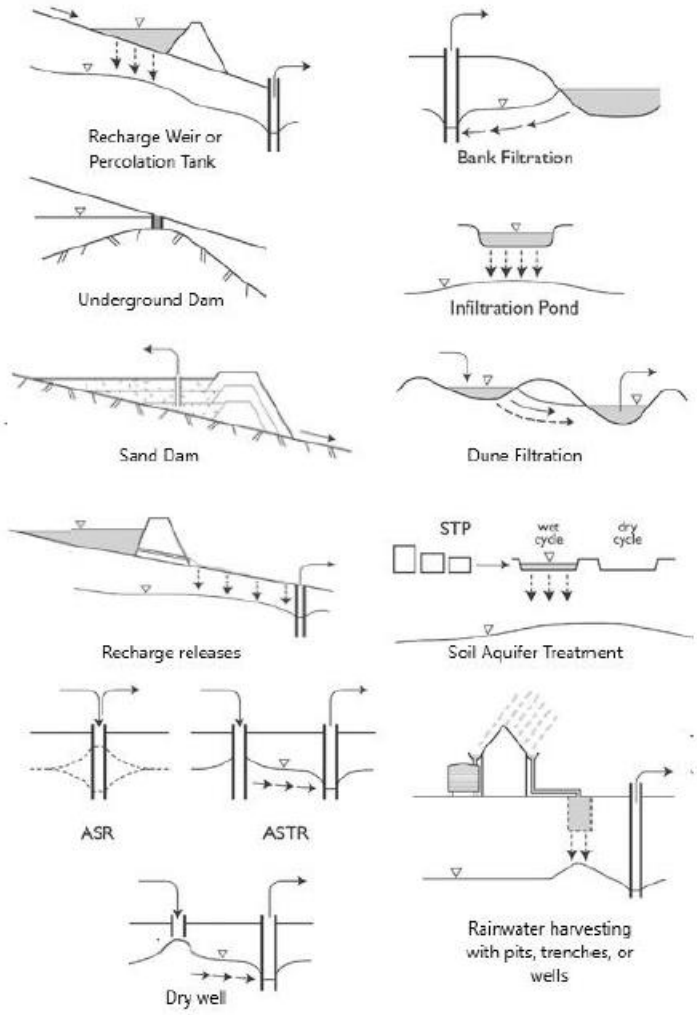

Figure 2. Schematic of different types of MAR. (ASR is Aquifer storage and recovery, ASTR is Aquifer Storage Transfer and Recovery (Dillon et al, 2022).

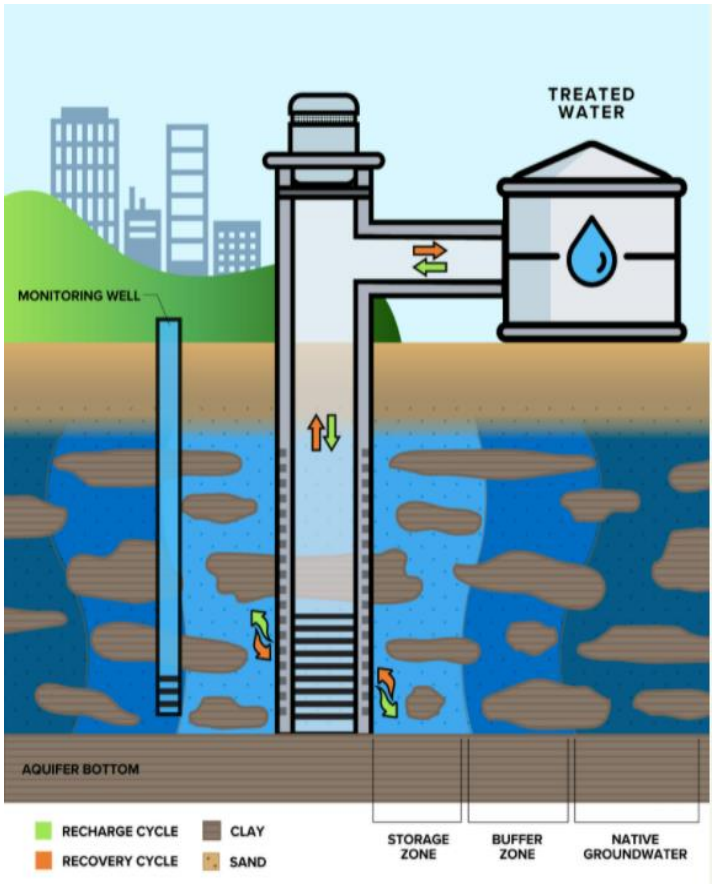

Figure 3. Schematic diagram of an ASR (adapted from Texas Water Development Board' website, 2022)

A few research articles involving the use of physical and numerical groundwater models as tools for evaluating the appropriateness of aquifers for the deployment of MAR systems are available. Here we will present to you some of the studies done with MAR and ASR-type MAR Most modeling studies relate to the injection of water into freshwater or into saline aquifers (Lowry & Anderson, 2006; M.J. Streetly, 1998; Yobbi, 1996). In the study of Kourakos et al., (2019), the authors use a large-scale integrated groundwater–surface water model that spans the entire CV of California, USA, to evaluate various Agricultural-MAR (Ag-MAR) practices (such

as varied recharge locations, quantities, and timings). The long-term effects of Ag-MAR on groundwater storage, surface and groundwater return flows, and instream flows are assessed at the local and regional levels using the numerical modeling framework. The findings demonstrate how important it is for Ag-MAR systems that stream water is generally available for recharge. Alam et al., (2020) used a coupled surface water and groundwater simulation model, to calculate the potential for groundwater overdraft recovery by MAR. The authors simulated water allocation scenarios where streamflow over the 90th or 80th percentiles was reallocated to aquifers in order to assess the potential advantage of MAR, subject to limitations on the maximum depth of applied water. The authors used the coupled surface water–groundwater model to do this (0.61 and 3.05 m). MAR, according to our findings, could, based on a 56-year calculation, recover 9 to 22 percent of the current groundwater overdraft CV-wide (1960–2015).

Kimbler (1970) used physical laboratory models for simulation of ASR (Kimbler, 1970). Pavelic et al. (2005) used FEFLOW software (Finite Element subsurface FLOW system) to perform numerical simulations to evaluate the dynamics of the injected water from different ASTR wells with different scenarios at Salisbury, Australia. Bakker et al., (2010) developed a numerical model to assess the recovery efficiency of ASR wells located in a saline aquifer. Ward et al. (2009) developed a predictive method based on dimensionless parameters reflecting lateral flow, dispersive mixing, mixed convection, and free convection to reduce the need for complex data from numerical groundwater models utilized in ASR injection investigations inside brackish groundwater aquifers. In Ward's approach, data on vertical and horizontal hydraulic conductivities (k), aquifer thickness, hydraulic gradient, and density of injected and ambient water are required.

ASR is often a seasonal storage operation that outperforms other solutions in terms of cost per unit of peak production capacity, i.e. \$/MGD or \$/m^3/d, for water to be available whenever needed. ASR is often less than half the price of other solutions when assessed on this basis (Snyder et al., 2022). While ASR has proven to be a cost-effective and efficient method of storing "excess water" in other states, previous studies show that Texas is behind in the implementation of ASR. Pirnie et al, 2011 summarized the current ASR systems in Texas and its capacities (Table 1).

Table 1. Operational capacity of current ASR in Texas (Pirnie et al. 2011)

Component	SAWS (60 mgd)	Kerrville (2.65 mgd)	EPWU (10 mgd)
Date	2004	1995	1985
Source Water	Groundwater	Treated River Water	Treated Wastewater
Storage	400-600 feet Carrizo	495-613 feet Lower Trinity	300-835 feet Hueco Bolson
Issues	• Single pipeline • Distribution system limitations	• Litigation during permitting • Lack of source water	• Original well design • Customers for reclaimed water
Expansion Plans	Part of 50-year Management Plan Evaluating TSV	Adding 3rd ASR well WTP; expansion in Regional Plan	Expanding FHWRP; Constructing 4th spreading basin

One of the distinct advantages of ASR is the associated environmental benefit (Pyne, 1995). Aquifer storage and recovery systems can serve as an alternative to surface reservoirs (TWDB, 2012). ASR has three major advantages that associated with evaporation, inundation, and sedimentation (Webb, 2015). One of the only two disadvantages (Webb, 2015) is if water is stored in an aquifer with native groundwater containing less than 10,000 milligrams of total dissolved solids, the injected water must be treated later to meet primary drinking water standards. This raises the cost of aquifer storage and recovery, particularly for purposes such as irrigation or power plant cooling that requires potable water. 2021 Rio Grande Regional Planning Group report (2020) rated ASR as a highly reliable water management with a reliability score of 5 out 5. Strategy that could potentially impact the local habitat due the area needed for the

implementation. Flat hydraulic gradients are uncommon in Texas, particularly in shallow aquifers. However, Chowdhury and Mace (2007) mentioned that groundwater levels in the Chicot Aquifer steadily drop to near sea level in the central Cameron, Willacy, and Kenedy counties. Hydraulic gradients in the Evangeline Aquifer are steep in eastern Starr and Jim Hogg counties and flatten significantly in eastern Hidalgo and Brooks counties.

Groundwater modeling

Any instrument that approximates a field scenario is referred to as a model. Physical models, such as laboratory sand tanks, are used to physically replicate groundwater flow. A mathematical model indirectly mimics groundwater flow using a governing equation that is assumed to represent the physical processes that occur in the system, as well as equations that define hydraulic heads or water flows along the model boundary conditions (Anderson & Woessner, 1991). Computer models of groundwater systems simulate groundwater movement, which include water levels, chemical particle transport, and thermal energy. Groundwater models (Fig. 4) provide a framework for hydrologists to organize their knowledge and understanding of groundwater systems. Models also can provide the information water managers need to plan efficiently for future water demands (Provost et al., 2009).

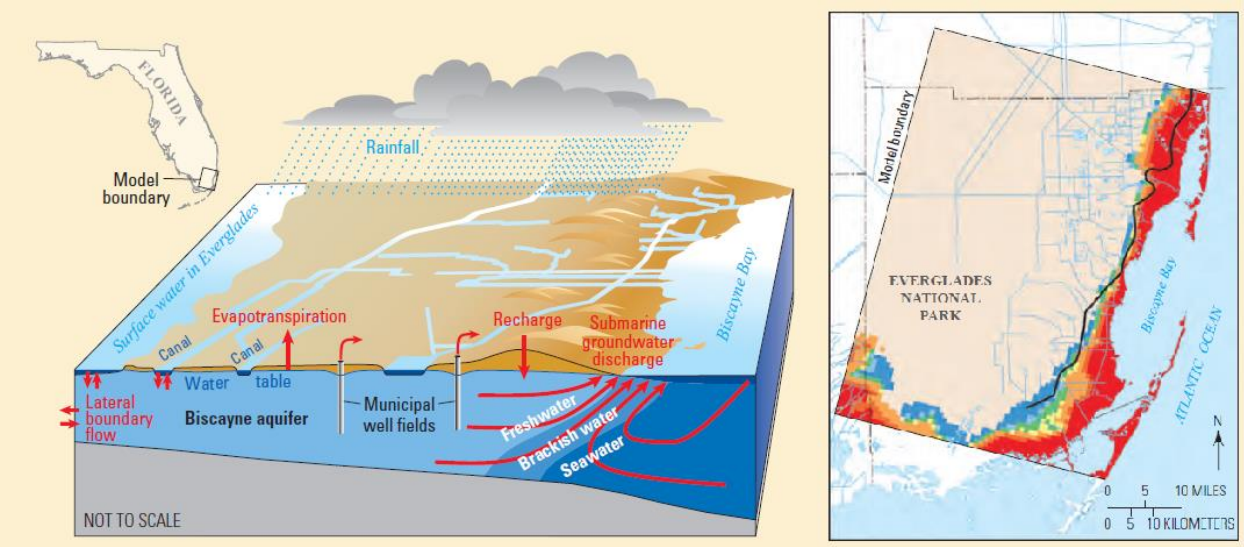

Figure 4 Groundwater model. A computer model (left) that replicates ground-water salinity in the coastal aquifer is based on a conceptual model (right) of groundwater flow to Biscayne Bay, Florida. The shift from freshwater (tan) to ocean (blue) is depicted on the map by the colors (red) (Provost, 2009).

The majority of groundwater modeling tries to forecast the outcomes of future action or hydrologic conditions. However, models are also used to re-create past conditions and also as interpretive tools. Interpretative uses include: (1) engineering calculators, which provide a quick answer to a specific engineering question; (2) screening models which assist the modeler in developing an initial understanding of a groundwater system and ‘or testing hypotheses about the system; and (3) generical models, which investigate processes in generic hydrogeologic settings. Engineering calculator models and generic models are typically not calibrated. Calibration of screening models is optional (Anderson et al., 2015).

When it is determined that a numerical model is required and the purpose of the modeling effort is clear, the model design and application process can begin. The modeling procedure includes steps, such as code selection and verification, model design, calibration, sensitivity analysis, and prediction (Fig 5). Each of these steps contributes to the demonstration that a given

site-specific model is capable of producing meaningful support, i.e., that the model is valid (Anderson et al., 2015).

This modeling workflow follows the approach in the scientific method shown in Fig 6. In the scientific method, a question is posed, a hypothesis is developed and tested, and the hypothesis is either accepted or rejected. If the hypothesis is rejected, the testing procedure is repeated with a revised hypothesis. Similarly, the groundwater modeling workflow begins with a question. Modeling should never be used as a mean to an end. A model is always intended to answer a specific question or set of questions. Although not depicted in the figure, field data and soft knowledge (i.e., any information that is not directly evaluated by model output) influence almost every step of the modeling process, particularly conceptual model design, parameterization, calibration target selection, and calibration process termination (Anderson et al., 2015).

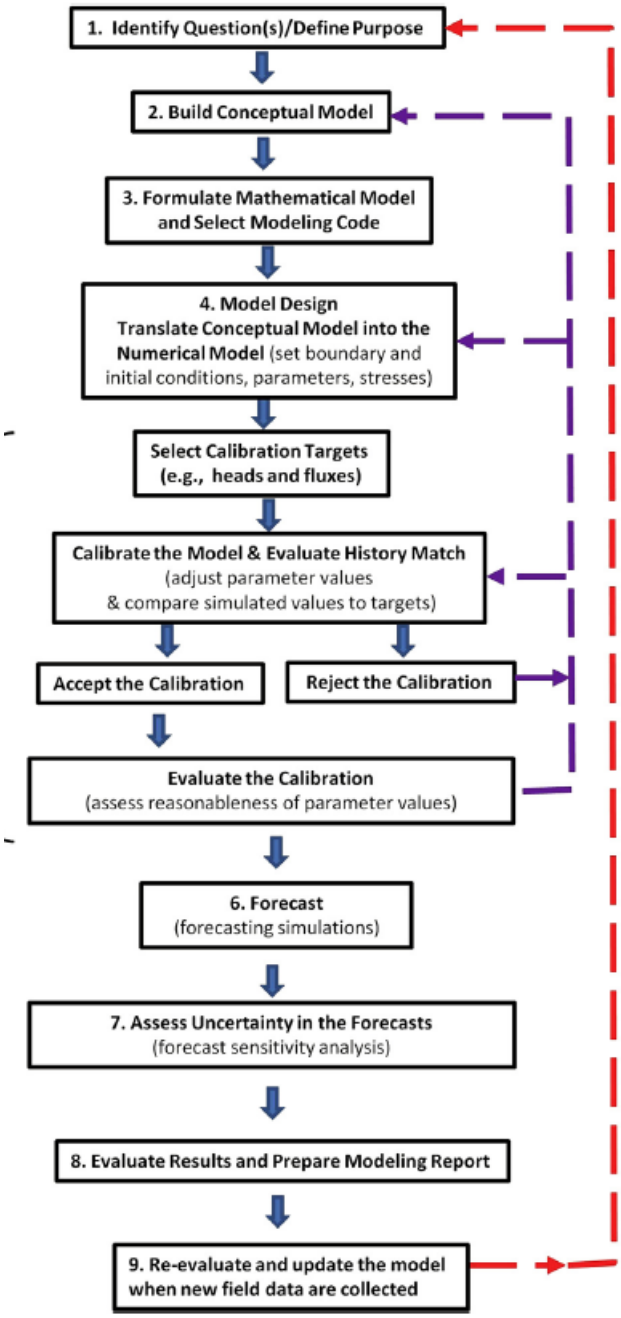

Figure 5. Standard groundwater modeling workflow (adapted from Anderson et al., 2015)

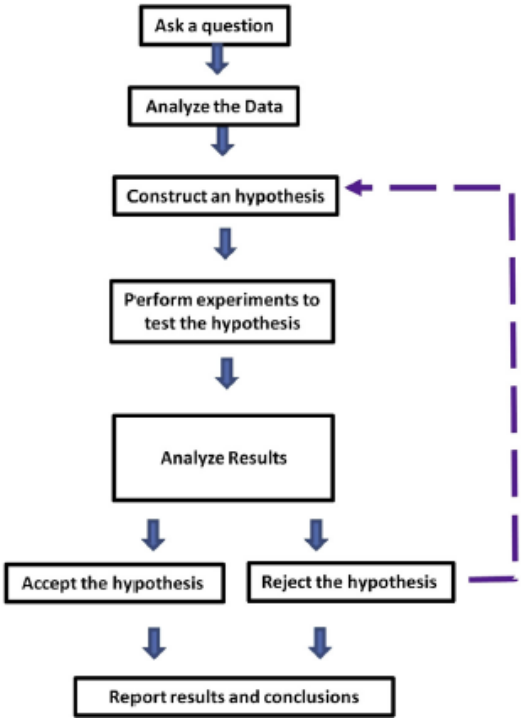

Figure 6. Scientific method flow chart (adapted from Anderson, 2015).

The governing equation

Two fundamental principles serve as the basis for process-based groundwater flow models. Darcy's law states groundwater flows from high to low potential energy; while the conservation of mass states water is neither created nor destroyed (equation 1.0). A mathematical model for groundwater flow consists of a governing equation (derived from conservation of mass and Darcy's law) that represents processes within the problem domain, boundary conditions that represent processes along the boundaries, and initial conditions that specify values of the dependent variable (i.e., hydraulic head) at the start of the simulation for time-dependent (transient) problems (Anderson et al., 2015)

$$\frac{\partial \rho}{\partial t} + \nabla(\rho v) = 0$$

(1.0)

Simplifying assumptions are unavoidable when representing hydrogeologic processes mathematically. The governing equation incorporates these assumptions. The form of the governing equation derived below is the most commonly used in groundwater flow modeling. Darcy's law is used to represent the flow of a single-phase fluid (water) at constant density in a continuous porous medium.

A general flow equation for two-dimensional profile or in three dimensions for unconfined aquifer and confined aquifer is shown in equation 1.2 and 1.3, respectively.

$$\frac{\partial}{\partial x}(K_x h \frac{\partial h}{\partial x} + \frac{\partial}{\partial y}\left(K_y h \frac{\partial h}{\partial y}\right) + \frac{\partial}{\partial z}\left(K_{yz} h \frac{\partial h}{\partial z}\right) = S_y \frac{\partial h}{\partial t} - R$$

(1.2)

$$\frac{\partial}{\partial x}(T_x \frac{\partial h}{\partial x} + \frac{\partial}{\partial y}\left(T_y \frac{\partial h}{\partial y}\right) + \frac{\partial}{\partial z}\left(T_z \frac{\partial h}{\partial z}\right) = S_s \frac{\partial h}{\partial t} - R$$

(1.3)

Where S_y is specific yield and R is recharge rate., S_s is for specific storage, T is for transmissivity, and K is hydraulic conductivity. Here, head (h) is equal to the elevation of the water table measured from the base of the aquifer (Anderson et al., 2015; Anderson & Woessner, 1991).

Numerical model

Analytical solutions to partial differential equations (PDE) cannot handle complex real-world problems because they require many assumptions, simplifications, and estimations that do not exist in reality. To deal with the complexities of groundwater systems, numerical methods were developed. Numerical models are made up of numerical solutions to a set of algebraic equations at discrete head values at specific nodal points (Baalousha, 2008).

To calculate head at specific locations, numerical models employ an approximation of the governing equation. A numerical solution is not continuous in space or time; head is calculated at discrete points (nodes) in space and for specified time values in contrast to analytical solutions. Under complex boundary and initial conditions, numerical models can solve the full transient, 3D, heterogeneous, and anisotropic governing equation.

The finite-difference method (FDM) and finite-element method (FEM) are the most commonly used numerical methods in groundwater modeling (Baalousha, 2008; Anderson et al., 2015). The FDM locates nodes in 3D space by assigning relative locations within a rectangular grid using indices (i,j,k). The FEM designates node locations in a mesh using spatial coordinates (x,y,z).

Figure 7(a) Horizontal two-dimensional (2D) FD grid with uniform nodal spacing; I = columns and j = rows. Occasionally, a different indexing convention is used. In MODFLOW, for example, there are I = rows and j = columns. The cells are block-centered, and the problem domain is represented by a thick dark line. Inactive cells (those located outside the problem domain) are shaded. Figure 7(b) shows the 2D horizontal FD grid with notation for the group of

five nodes that comprise the FDM computational module (star) centered on node (i,j). Figure 7(c) Three-dimensional notation in which Δz denotes the vertical distance between nodes and k denotes the vertical index. The group of blocks on the right is depicted in two dimensions (the two blocks perpendicular to the page along the y-axis are not shown). The FD computational module in three dimensions is made up of seven nodes, including nodes (i,j,k) boundaries (Anderson, et al., 2015).

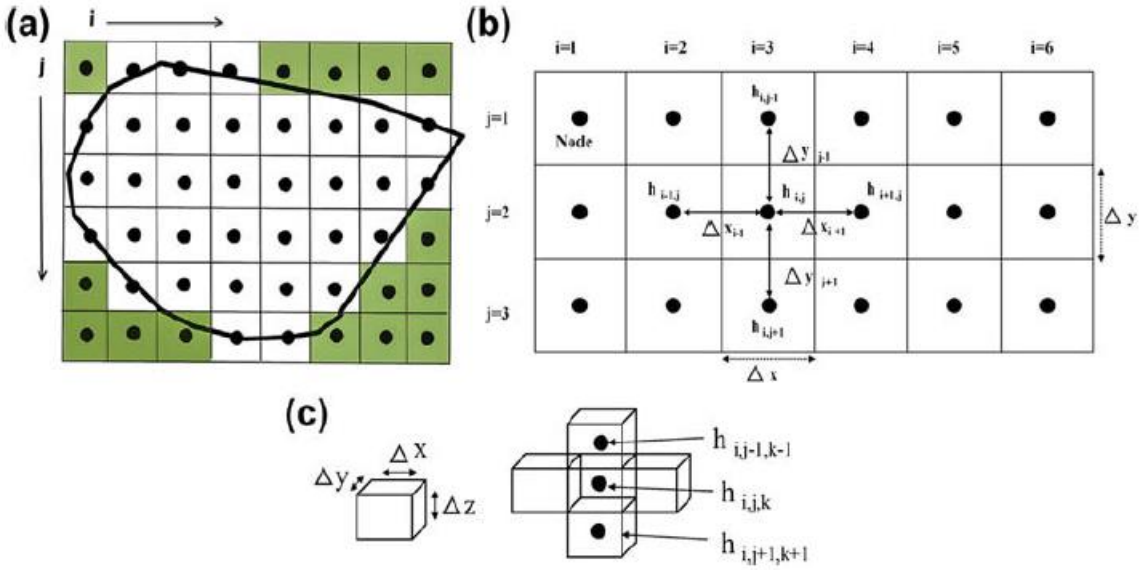

Figure 7. Grid and notation for finite-difference (FDM) (Anderson, et al., 2015).

The FEM designates node locations in a mesh using spatial coordinates (x,y,z). The problem domain is subdivided into elements defined by nodes in the FEM (Figure 8.). In contrast to the FDM, where head is defined only at the nodes and is considered piecewise constant between nodes the dependent variable (e.g., head) is defined as a continuous solution within elements (Anderson, et al., 2015).

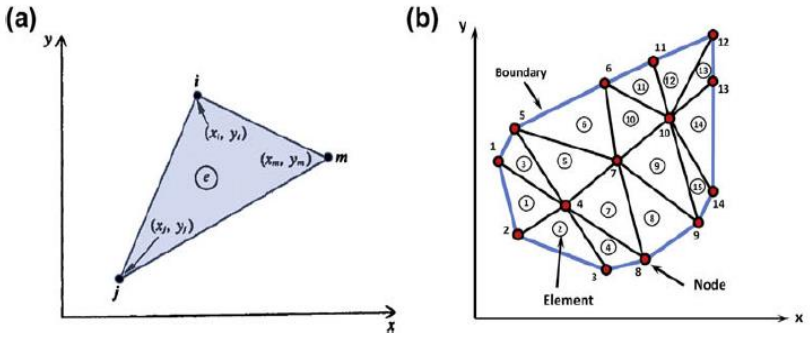

Figure 8. Horizontal two-dimensional finite-element mesh with triangular elements and symbols. (a) A example triangle element with nodes i, j, and m labeled in counterclockwise order, with spatial coordinates (x,y); (b) Triangular elements are defined by numbered nodes, with element numbers inside circles. The elements are shaped to fit the issue domain's boundaries (Anderson, et al., 2015)

Groundwater model

MODFLOW-2005 is a version of the MODFLOW finite-difference ground-water model. MODFLOW employs a modular framework in which comparable program operations are grouped together and specific computational and hydrologic options are built so that each option is independent of the others. Because of this structure, new options can be added without having to change old ones. The model can be utilized for two-dimensional or three-dimensional applications. Input processes have been created in such a way that each form of model input data can be stored and read from a different external file (Harbaugh, 2005). Recharge, evapotranspiration, areal recharge, flow to wells, flow to drains, and flow to riverbeds are all simulated by the model. It is built up as a collection of independent modules; the user selects only the modules required for the specific system under examination (Fetter, 2000).

MT3DMS, where MT3D stands for Modular 3-Dimensional Transport model and MS stands for multi-Species structure to accommodate add-on reaction packages. For simulating

advection, dispersion/diffusion, and chemical reactions of pollutants in groundwater flow systems under general hydrogeologic conditions, MT3DMS provides a broad set of options and capabilities.

Groundwater availability of Gulf coast aquifer in Lower Rio Grande Valley

Groundwater availability or flow models are an excellent tool for assessing groundwater availability and the effects of water management techniques under a variety of climatic circumstances. A groundwater availability model is a numerical description of the aquifer system that can simulate historical conditions and anticipate future aquifer conditions using different pumping and climate scenarios (Shi et al, 2020). Multiple versions of groundwater availability or numerical models that cover the southern part of the Gulf coast aquifer are readily available from Texas Water Development Board websites. Chowdhury and Mace (2007) developed a model of the Gulf coast aquifer with four hydrostratigraphic layers (Chicot, Evangeline, Burkeville, and Jasper). The model contained a steady-state period simulating aquifer conditions prior to 1980, as well as a transient period from 1981 to 1999 (Chowdhury and Mace, 2007). During calibration, a number of cells went dry and these cells were made inactive after observing the aquifers are too thin in this area (Chowdhury and Mace, 2007).

In 2011, Hutchison and others developed a groundwater flow model using a three-dimensional MODFLOW–2000 that includes the extent of Groundwater Management Area 16 and its underlying aquifer systems resulting in a total of six modeled layers. These includes the Gulf Coast aquifer system from Chowdhury and Mace (2007), Layer 5 represents the Yegua-Jackson Aquifer System, which includes sections of the Catahoula Formation, while Layer 6 represents the Queen City, Sparta, and Carrizo-Wilcox Aquifer Systems. This model also

includes a steady-state period from pre-1963 conditions and transient conditions from 1963 through 1999.

Shi and others of TWDB (2020) created a conceptual groundwater model encompassing groundwater management area 15 and 16. This conceptual model serves as the basis for a numerical groundwater availability model (Shi et al., 2020). Updating models developed previously, the stratigraphic units used in Shi et al. (2020) are classified into four hydro-stratigraphic units, the Chicot aquifer as Layer 1, Evangeline aquifer as layer 2, Burkeville confining unit as layer 3 and lastly, Jasper aquifer as layer 4 (Shi et al., 2020).

Additionally, a groundwater transport model was developed (Panday et al. 2017) using a three-dimensional MODFLOW USG flow and transport model to simulate variations in groundwater levels, concentrations of total dissolved solids (TDS), and surface-water/groundwater interactions. To assess the effect of salt density on groundwater flow and solute migration, the model includes density dependent flow. A total of 12 numerical layers were used in the model, where layers 1-10 represent the Gulf Coast Aquifer system . The Gulf Coast Aquifer System was reproduced as Layers 1 through 10 of the models (Beaumont, Lissie, Willis, Upper Goliad, Lower Goliad, Upper Fleming (Lagarto), Middle Fleming (Lagarto), Lower Fleming (Lagarto), Oakville, and Upper Catahoula formations). The grid of the model (1 mile by 1 mile.

Desired future conditions

TWDB is tasked with developing a long-term flexible and comprehensive strategy for the development, conservation, and management of the state's water resources. Historically, the TWDB created the State Water Plan (SWP) with participation from other state and local

agencies, as well as the public. The 75th Legislature enacted Senate Bill 1 (SB1) in 1997, which instituted a "bottom up" system in which SWPs are based on regional water plans (RWPs) prepared and adopted by the 16 designated Regional Water Planning Groups (RWPGs) (2021 Rio Grande Regional Planning Group 2020). The purpose of the state's water planning strategy is to provide adequate water supply for all Texans during times of drought. Texas has a long history of drought. There is no sign that this trend will change. In fact, recent droughts remind us that more severe drought conditions are likely to occur at some point in the future. (Paup, 2021) In CMIP5 (Coupled Model Intercomparison Project Phase 5) mean forecasts, Ventakarama et al. (2016) discovered increased drought frequency and severity in Texas toward the latter half of the 21st century.

The RWPs are updated every 5 years and an updated SWP is issued after a year of their adoption. RWP covers planning horizon from 2020 to 2070. The RWPGs collaborate with the TWDB to assess current water consumption and forecast future water demands for each Water User Group (WUG): municipal, irrigation, livestock, steam-electric power generation, manufacturing, and mining. Measured amounts, conservation goals, and modeling are combined to create availability data for all major water resources, indicating how much water can be relied on in a drought year while staying within each resource's management goals.

The currently available water resources are examined and anticipated for each WUG over the planning horizon. Future needs are estimated and measured by comparing reliable, drought-year supplies to drought-year requests. The creation of suggestions for water management techniques is driven by these estimations for needs (WMSs). WMSs include methods for reducing demand, increasing supply, and minimizing losses (2021 Rio Grande Regional Planning Group, 2020).

Population centers in Region M are depicted in Figure 9 as well. The region's population is predicted to exceed 4 million by the conclusion of the current planned horizon, representing a 106 percent growth from 2020 to 2070. The population of Region M is concentrated in Cameron, Hidalgo, and Webb counties, which account for 90.5 percent of the regional total in 2010. The US Census Bureau estimates Region M's total population in 2013 to be 1,237,942, up 4.8 percent from 2010 (compared to 5.2 percent growth statewide). (2021 Rio Grande Regional Planning Group, 2020).

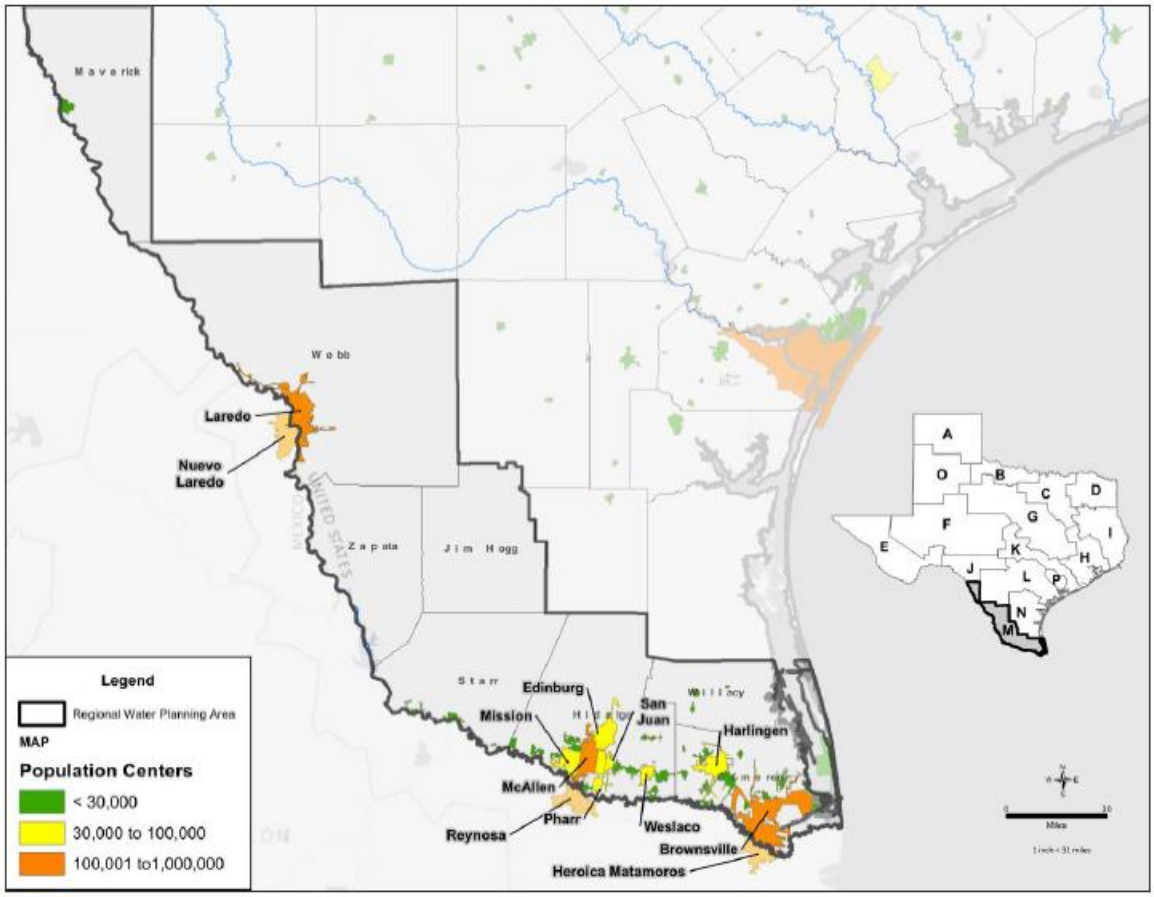

Figure 9. Region M counties and population centers (2021 Rio Grande Regional Planning Group, 2020).

CHAPTER III

MATERIALS AND METHODS

Study area

The study area for this research is located primarily in the Lower Rio Grande Valley in South Texas. The area is comprised of portion of Jim Hogg, Brooks, Kennedy, Starr, Hidalgo, Willacy, and Cameron County (Schorr et al., 2017) that sits on top the Gulf Coast Aquifer (Meyer et al., 2014). Furthermore, the research area encompasses the southern portions of Groundwater Management Area 16 Groundwater Flow Model by Hutchison, et al.,(2011). The Gulf Coast Aquifer System in the study area occupies 7570.26 square miles in 7 counties. The model boundary extent itself is based on the Burkeville boundary used in Conceptual model report by Schorr et al. (2017)

The Gulf Coast Aquifer was found to be one of the aquifers most suitable for ASR and has suitability ratings of more than 0.85 according to a recent TWDB (2020) report (Fig. 9). The grid cells found in Laredo, Hidalgo, McAllen and Pharr are among the cities that are found to have the ideal hydrogeologic characteristics (hydraulic properties), excess water and water supply need scores. The selected ASR wells locations were chosen based on permeability of the layer and closest desalination plants, identified from the LRGV GAM and LRGV Transport model.

The TWDB also indicated that low suitability in this assessment (Fig. 9) does not necessarily imply that the aquifer is not suitable, but rather less preferred compared to other regions in the state based on multiple rating factors (e.g., demands, water supply, and hydraulic properties). Final Suitability Ratings were combined from these parameters to help identify the areas where suitable hydrogeology, excess water, and water needs. Figure 10 (TWDB, 2020) indicated ASR Suitability Rating by grid cells (50,000 ft by 50,000 ft) as "less"," moderately", and "most" suitable. More details regarding rating approach, methodology, analysis completed at each screening criteria can be found in TWDB report (2020).

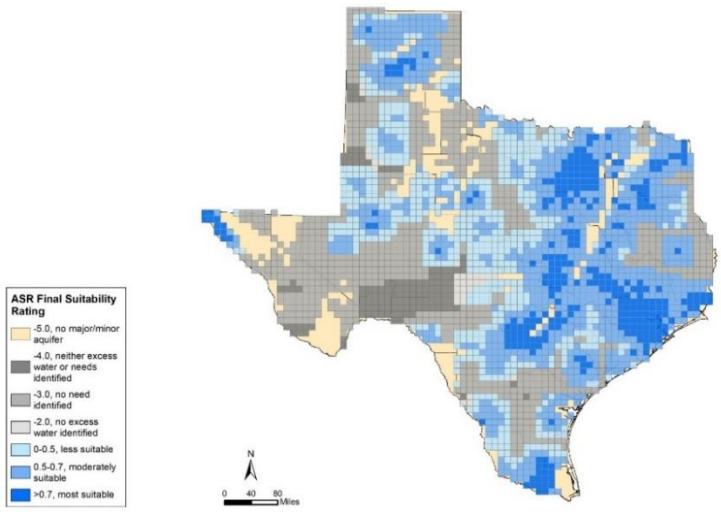

Figure 10. Final ASR suitability rating. Each parameter screenings are classified as "low", "medium" or "high" suitability (TWDB, 2020).

Hydrogeology

The study area is located at Lower Rio Grande Valley of South and covers the county of Hidalgo, Cameron, Kennedy, Brooks, Willacy, and Jim Hoggs (Chowdhury & Mace, 2007). Gulf Coast aquifer serves as the primary aquifer in this region. It is divided into four aquifers the Chicot, Evangeline, Burkeville, and Jasper Aquifers, which are made up of discontinuous sand, silt clay and gravel beds of Miocene to Holocene age (Figure 11). From the Gulf of Mexico in the East, the Lower Rio Grande Valley is a flat plain that extends to the Bordas Escarpment in the West that rises up to 500 feet in Starr County. Near the southern edge of the escarpment, the plain slightly dips southeastward (Chowdhury & Mace, 2007). This study will partly honor the hydrostratigraphic model in Figure 12 which is from the LRGV Transport model (from top to bottom): Chicot, Evangeline, and the Burkeville confining unit. Each aquifer will also be subdivided into its individual geologic unit. Surficial layering of the model area is shown in Figure 13. This research Only Layer 1-7 in the figure were considered in this study. Additionally, water qualities differ with depths and locations. The Gulf coast aquifer in the South is more saline (1,000 ml/L – 10000 ml/L) (S-S' in Fig. 11) compared to the central and northeastern parts of the aquifer (<500 ml/L) (N-N' in Fig. 11). The stretch of the aquifer along the Gulf coast is defined by the dipping of freshwater, the sedimentary units that makes up the aquifer becomes more saline below the Gulf of Mexico (Bruun et al., 2016). Within the portion of Gulf Coast aquifer in LRGV (S-S' in Fig. 11), there are still variations in salinity (TWDB, 2017)

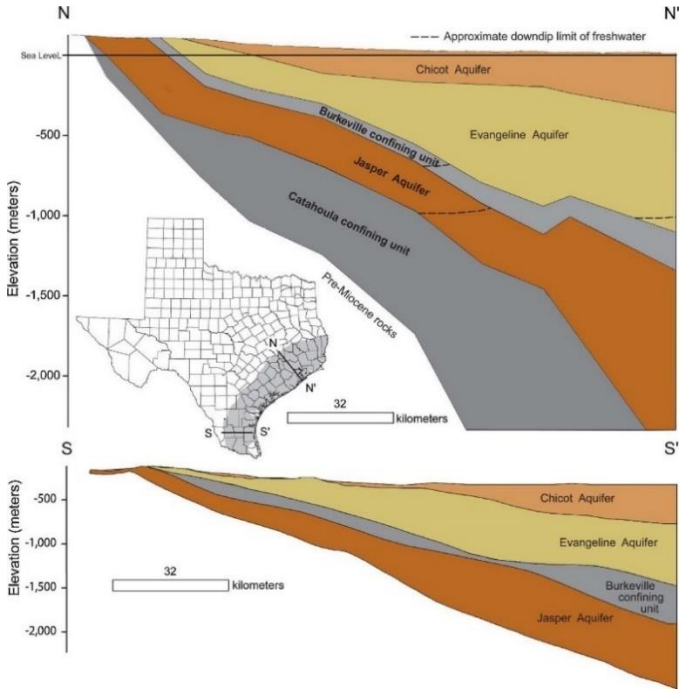

Figure 11. Cross section of the Gulf Coast aquifer system (Smith et al., 2017*)*

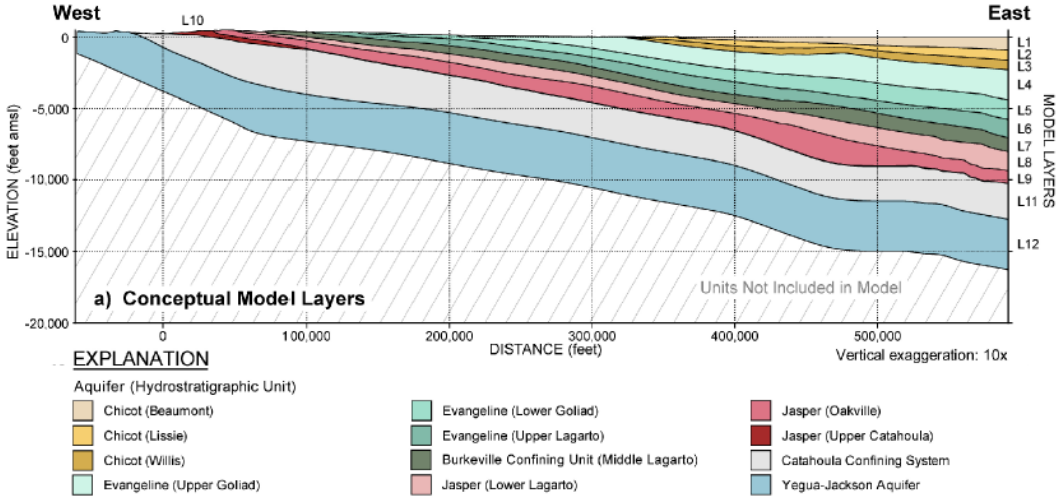

Figure 12. Conceptual model layers from 2017 Transport model. (Panday et a., 2017).

The layering of aquifers and related confining units in a research region is referred to as hydrostratigraphy. The elevation surfaces of the top and bottom of the hydrostratigraphic units in

chronostratigraphic order make up the hydrostratigraphic framework of an aquifer system. The Chicot aquifer comprise of Beaumont, Lissie, and Willis formations are composed mainly of clay-rich sediments cut across by sandy fluvial and deltaic-tributary channel deposits, sandy clay and fine-grained sand, and several upward-fining sequences containing gravely coarse sand. Evangeline aquifer contains the Upper Goliad, Middle Goliad, and Upper Lagarto Formations. This aquifer has thick sequences of sand with some intervals of sand and clay. Lastly, the Burkeville Confining Unit divides the Evangeline and Jasper aquifers, and contains the Middle Lagarto, mainly composed of silt and clay with isolated lenses, and is identified to act as a confining unit (Schorr et al., 2017).

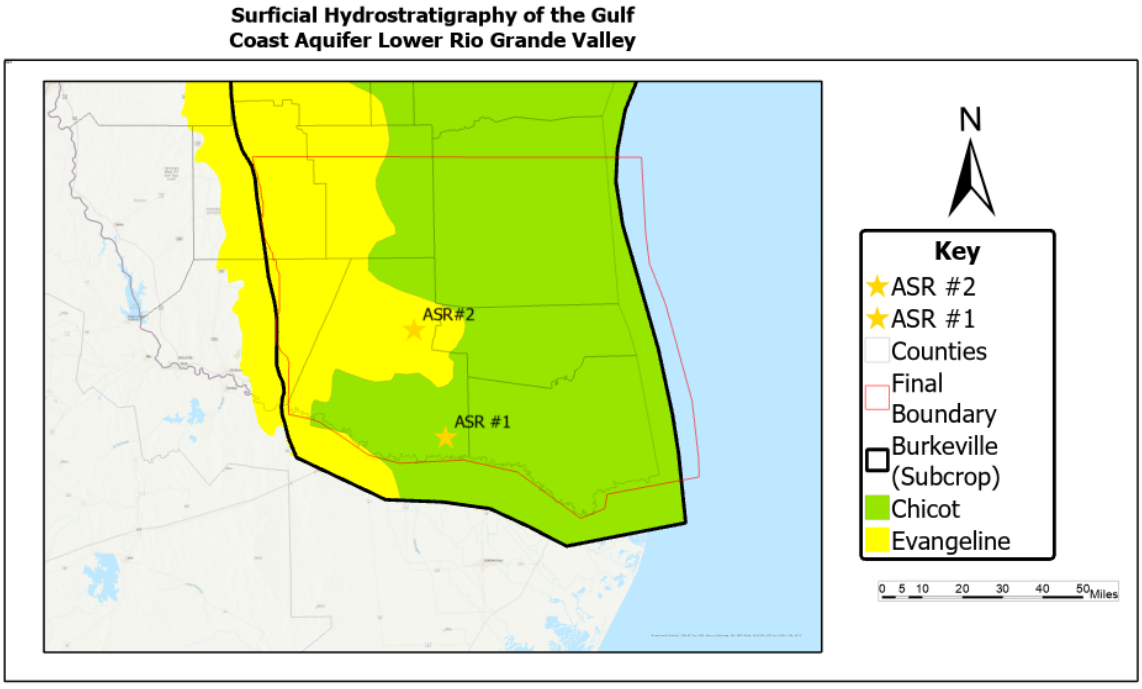

Figure 13. Outcrops of the target aquifers. Shapefiles were adapted from the LRGV Transport model geodatabes. (Panday et al., 2017).

Groundwater Levels and Flow

Regional Groundwater movement in the valley is mainly to the east from highland areas in eastern Starr and Jim Hogg counties to the Gulf of Mexico in Cameron, Willacy, and Kennedy counties, according to groundwater elevation contour maps (Chowdhury et al, 2007). Groundwater levels in central Cameron, Willacy, and Kenedy counties gradually drop to near sea level in the Chicot Aquifer. Hydraulic gradients in the Evangeline Aquifer are severe in eastern Starr and Jim Hogg counties and flatten significantly in eastern Hidalgo and Brooks counties (Schorr et al. 2017)

Water Availability

The study area is also a part of the region that is appointed as part of The 2021 Rio Grande Regional Planning Group Planning Group Water Plan Group (RGWPG M) which reports annually to the State Water Plan to provide the region's development, management, and conservation of water resources, as well as preparation for response to droughts. Region M draws most of its water from the Rio Grande River through the Amistad-Falcon Reservoir System watershed, which is jointly operated with Mexico (2021 Rio Grande Regional Planning Group Planning Group Water Planning Group, 2012). For residential and agricultural purposes, the research area has been linked to the Rio Grande's waters. Most years, the tropical or subtropical environment allows for an extended growing season. Rainfalls in the Lower Rio Grande Country vary from 28 inches at the coast to 18 inches in the northwestern part of the region, with thunderstorms in the spring and infrequent hurricanes in the late summer and fall being the main contributors. Because of the region's relatively flat geography, these storms can produce massive volumes of rainfall in a short period of time, causing widespread flooding (2021 Rio Grande Regional Planning Group Planning

Group Water Planning Group, 2020a). Other Potential sources of surface water stated by Khan et al. (2007) and by TWDB's Statewide Survey Aquifer Storage (Shaw et al., 2020):

- Flood mitigation (extra water)
- River flows (during high flow seasons) result in an effective increase in en-route storage capacity, allowing for improved efficiency, control, and flexibility in water management.
- Replacement or replenishment of present en-route storage (as well as a reduction in evaporation losses), as well as
- Sewage treatment plants.

If appropriately developed, a groundwater flow model without density simulation can still be a valuable tool for identifying the paths and travel periods of brackish, saline, and brine waters (Shi et al, 2020; Anderson et al., 2015).

The numerical groundwater model

To assess the capabilities of implementing MAR systems at a specific site at Lower Rio Grande Valley to help water demands and flood control, a numerical groundwater model will be developed to simulate the performance of an MAR system in LRGV. The ASR system at the specific-site study was modeled using a 3-D graphical user interface Visual (VMOD) Flex (Version 7; Waterloo Hydrogeological, Ontario, Canada).

This modeling study consists of four major tasks. First, The hydrogeological frameworks and formations were conceptualized into regional conceptual model under the VMOD to create the 3-D numerical model grid. This modeling study includes the Chicot aquifer (Layer 1-3) , the Evangeline aquifer (layer 4-6), and the Burkeville Confining unit aquifer (Layer 7). Each aquifer was further subdivided into sub-aquifers (7 model layers). The second task was to specify the

aquifer properties into the model domain, which includes mainly the hydraulic conductivity, specific storage, specific yield, and porosity. The third task is to assign the boundary conditions such as the river (major canals), recharge, evapotranspiration, groundwater pumping. The fourth task is to assign a well or a well nest that will act as an ASR system in modeling domain.

The overall domain of the model is shown in Figure 14. This model domain is based on the west extent of the Burkeville aquifer of previous LRGV Transport model (Panday et al., 2017) and the Groundwater Availability Model (GAM, Chowdhury and Mace, 2007). The model is made up of seven layers, total of 90 rows and 112 columns. The length and width of the cell are 5,280 feet (one mile by one mile). English units were used in this model, e.g., feet, miles.

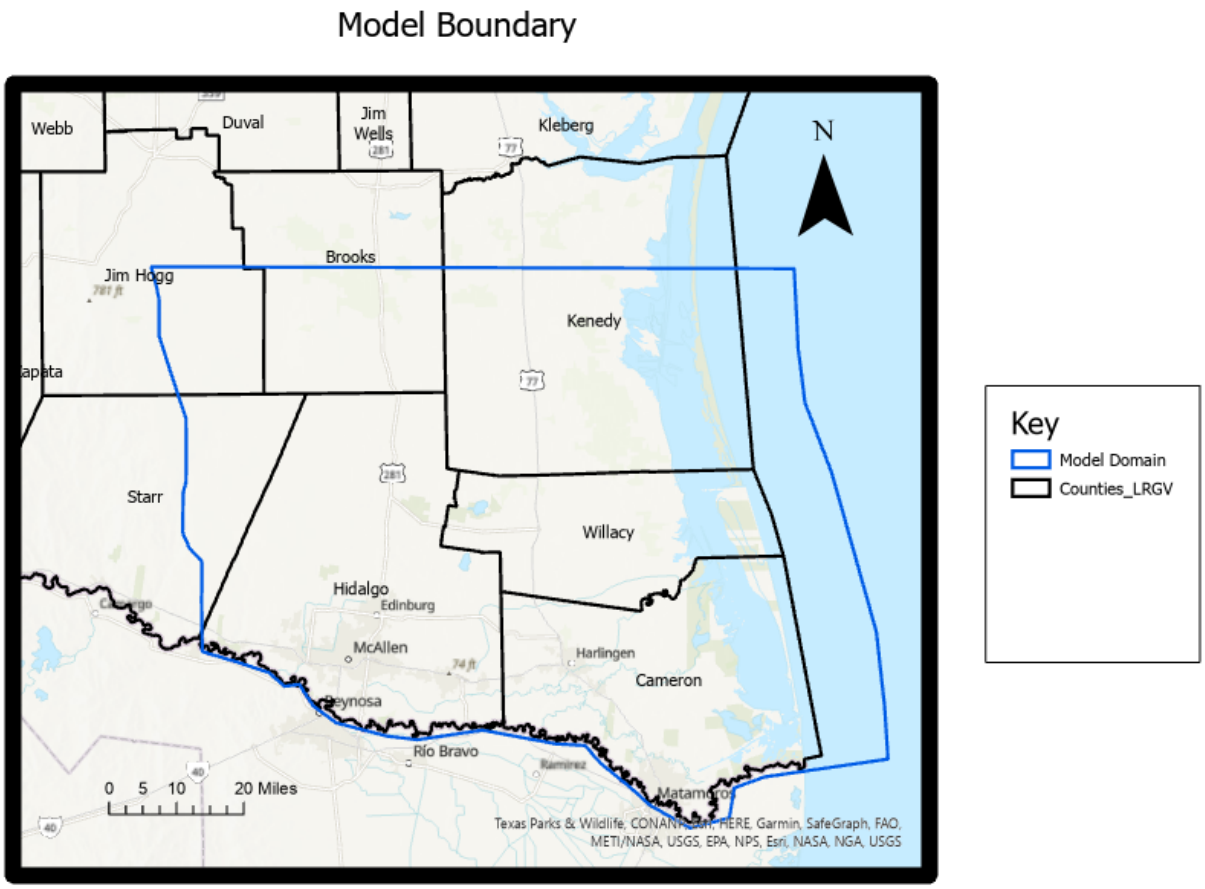

Figure 14. Proposed model domain boundary.

Modeling development

This study followed a similar modeling project conducted by Chowdhury and Mace of TWDB (2007). First, a steady state model will be created and calibrated with available data. Secondly, a transient model will be calibrated. At last, the injection wells will be added to the calibrated transient model to predict water levels and improve the overall water budget. Matching water levels under steady-state conditions and seasonal water level changes under transient conditions is the method for calibrating the model. To calibrate the model, Chicot and Evangeline aquifers were used as the targets, which will have greatest number of wells (treated as control points in the model).

The numerical groundwater-flow model was developed to simulate the envisioned groundwater-flow system under steady-state, 1984 conditions, and transient conditions, with annual stress periods ranging from 1985 to 2014. This time period was chosen primarily because to the available data from pumping and water levels. Also, it includes time before and after the initiation of brackish groundwater desalination activities in the LRGV (Panday et al., 2017).

Materials to develop the Conceptual Model

Anderson et al., (2015) defined a Conceptual model as a qualitative representation of a groundwater system that is based on geological, geophysical, hydrological, hydrogeochemical, and other necessary information and compliant to the hydrogeological principles. The hydrogeological conceptual model incorporates all of the research site's specific data and

background knowledge, to manage and represent the data domain and the behavior of the processes that drive water flow and solute transport (Mero et al., 2021).

Most of the hydraulic parameters (Table 2) and boundary (Table 3) inputs were extracted from multiple legislative and contracted reports from TWDB, which are Groundwater Availability Model (GAM) (Chowdhury and Mace, 2007), Groundwater Flow Model (Hutchison et al., 2011), Conceptual Model Report (Schorr et al., 2017), Solute Transport Model (Panday et al., 2017), Groundwater Management Area 15 and Draft Conceptual Model Report by (Shi et al., 2020).The bottom extent of each layers and top surface layers is shown in Figure 15. These layers were extracted from the geodatabase of Panday et al., (2017).

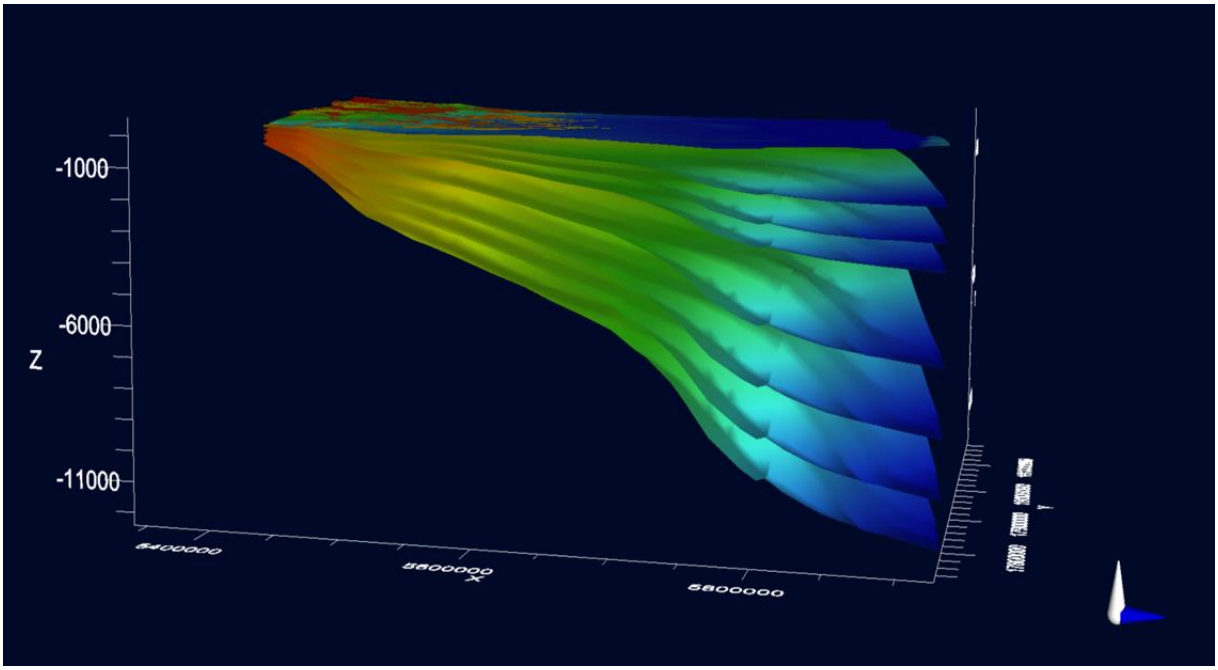

Figure 15. The bottom extent of each layer and the top surface layer**.**

Table 2. Model property parameters

Model Parameters	**Source(s)**
Elevations of the aquifers	GAM, LRGV Transport model
Horizontal and Vertical Hydraulic conductivity (K)	GAM, LRGV Transport model

Storage (specific Storage (Ss), Specific Yield (Sy), Total Porosity (Tp), and Effective Porosity (Ep)	GAM, LRGV Transport model

Table 3. Model boundaries

Boundaries	**MODFLOW package used**
Western Extent (General Head)	GHB
Bottom/South boundary (RGV)	RIV
East/Gulf (Constant head)	CHB
Recharge	RCH
Evapotranspiration	EVT
Pumping/Injection Wells	WEL

Code selection

The simulations will be performed using the built-in packages finite-difference MODFLOW 2005. MODFLOW output files and names are listed in Table 4

Table 4. MODFLOW-2005 packages

MODFLOW-2005 Package	**Abbreviation**	**Description**
Namefile	NAM	Controls model files and names.
Basic	BAS	Specify basic model and stress periods
Discretization	DIS	Discretizes groundwater area
Layer Property Flow	LPF	Runs aquifer properties
Connected Linear Network (Well Package)	WEL	Implement sources/sink
Recharge	RCH	Implement recharge
River	RIV	Implement River boundary
General Head Boundary	GHD	Implement head-dependent boundary
Evapotranspiration	EVT	Implement evapotranspiration
Constant Head	CHD	Implement Constant Head boundary

Basic package

The Basic (BAS) Package of the Groundwater flow (GWF) Process handles various task for MODFLOW. This package reads the Name File which contains input and output files. BAS package assigns memory for variable, reads active and inactive cells, read IBOUND variable, reads initial heads, tracks head throughout time, reads data specifying the discretization of time and space, solves for overall water budget, and controls model output specified by the user (Harbaugh, 2005)

Discretization package

The basic package specifies spatial and temporal discretization of the model from Discretization file (DIS), which is required from all model simulations (Harbaug, 2005). The model contains 90 rows and 112 columns. The cell length is 1 mile by 1 mile which is the same from TWDB 2007 and 2011 reports. The cell size was chosen to be small enough to reflect the density of input data and the required output detail while remaining large enough to allow the model to be manageable. We were able to easily manipulate the data using spreadsheets due to the uniform cell size.

Layer property flow

Hydraulic conductivity is the rate at which water can move through permeable media (Fetter, 2018). For each cell in the model domain, the Layer-property Flow Package gives the hydraulic conductivity and storativity values. We assigned layer 1, to be unconfined, and layer 2 – 7 to be unconfined/confined. This allowed the model to calculate transmissivity and storativity

based on saturated thickness. Hydraulic conductivity values were taken from Panday (2017) and Hutchison (2011) report. Table 5 shows the range of hydraulic conductivities for each layer.

Table 5. Hydraulic conductivity values

Layer number	Hydraulic Conductivities (Kx) in feet/day	Hydraulic Conductivities (Kx) in feet/day after calibration
Layer 1	0.1-800	0.367 – 402.15
Layer 2	800	0.367 - 800
Layer 3	0.1-50	0.367 – 25.5
Layer 4	0.1-28	0.367 – 2.55
Layer 5	0.1	2.55
Layer 6	11	7.03
Layer 7	0.001-200	0.066 - 10

Model boundary condition

Flows in and out of the groundwater system have been translated into the model boundary conditions using the boundary packages (Panday et al. 2017) of MODFLOW 2005. Model boundaries were assigned for recharge, pumping, rivers, outer boundaries and initial conditions.

Constant head

The constant head package was also employed to give a constant hydraulic head value of zero in layer 1 in the offshore parts of the domain (Panday et al, 2017). In the following layers, a no-flow border in the east to allow for upward vertical flow of water toward the coastline's discharge zones (Chowdhury and Mace, 2007).

General head

The general head boundary (GHB) package was used to simulate flow into the model domain from upstream lateral model boundaries. We assigned GHB boundary in the North and West side of the model. We used the interpreted water level from the Transport model (Panday et

al. 2017) to specify the GHB head. The boundary heads ranged from 500 ft to the northwest corner of the model to 100 ft to the south at Starr County, near the Rio Grande.

Recharge

On a regional scale, estimating groundwater recharge from precipitation infiltration is difficult. There has been research to enhance these estimations for the study area. Previous estimates of Gulf Coast Aquifer System recharge rates vary significantly due to differences in hydraulic conductivity, rainfall distribution, evapotranspiration rate, groundwater-surface water interactions, model grid cell size, and the presence of caliche in outcrop areas (Panday et al., 2017). For this study, we used the calibrated recharge rates from Panday et al., (2017) which are based on Scanlon and others (2012) chloride mass balance approach to estimate regional recharge throughout the Gulf Coast Aquifer System. Figure 16 shows the distributed recharge 1984 rates in Lower Rio Grande Valley for the steady state model. A scaling factor adopted from Panday et al., (2017) were also used for the recharge rates for different stress periods (Table 6). 2013 recharge rates were used for 2014 to 2018 stress periods.

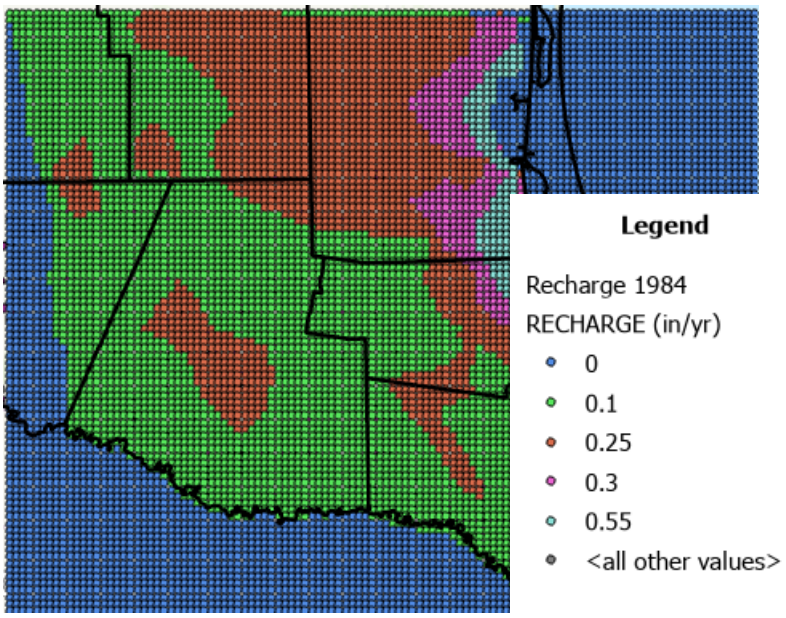

Figure 16. 1984 Recharge rate distribution (adapted from TWDB, 2017)

Table 6. Recharge multiplier for 1984 – 2018 conditions

Stress Periods	Representative Year	Recharge multiplier
1	1984	1
2	1985	1.19
3	1986	1.02
4	1987	1.23
5	1988	0.85
6	1989	0.65
7	1990	0.74
8	1991	1.28
9	1992	1.35
10	1993	1.25
11	1994	0.95
12	1995	1.12
13	1996	0.65
14	1997	1.29
15	1998	1.15
16	1999	0.97
17	2000	0.71
18	2001	0.86
19	2002	1.34
20	2003	1.58
21	2004	1.28

22	2005	0.82
23	2006	1.17
24	2007	1.39
25	2008	1.38
26	2009	0.92
27	2010	1.48
28	2011	0.55
29	2012	0.76
30	2013	1.13
31	2014	1.13
32	2015	1.13
33	2016	1.13
34	2017	1.13
35	2018	1.13

River

To simulate flow between the Chicot Aquifer and the Rio Grande, we used MODFLOW's River Package. The River Package makes use of river surface elevation, river bottom elevation, and riverbed sediment conductivity (Chowdhury and Mace, 2007). River heads were interpolated using rain gauges found in Anzalduas Reservoir, Rio Grande San Benito, TX, and at Brownsville, TX. This study also used Huthchison et al, (2011) rivers heads for the Rio Grande (Table 7).

The RIV package was also used to represent major irrigation canals and diversions from the Rio Grande as a river boundary (Table 8) condition in the model (Panday et al., 2017).

Table 7. RIV parameters for Rio Grande

Rio RIV Input	**Definition**	**Range**
River Stage	The elevation of the surface water. This elevation is subject to fluctuate over time.	0 - 120 (ft)
River Bed Bottom	The elevation of the bottom of the surface water body's seepage layer (bedding material).	-10 - 110 (ft)
Conductance	A numerical parameter representing the resistance to flow between the surface water body and the	1034813.61 - 113775139.93 (ft^2/day)

	groundwater caused by the seepage layer (riverbed).	

Table 8. Canal RIV parameter

Canal RIV input	Definition	Range
River Stage	The elevation of the surface water. This elevation is subject to fluctuate over time.	0 – 120 ft
River Bed Bottom	The elevation of the bottom of the surface water body's seepage layer (bedding material).	0-20 (ft)
Conductance	A numerical parameter representing the resistance to flow between the surface water body and the groundwater caused by the seepage layer (riverbed).	10.96 – 157.08 (ft^2/day)

Evapotranspiration

Evapotranspiration (ET) is the loss of water from a vegetated surface caused by the combined processes of soil evaporation and plant transpiration. Evapotranspiration rates are affected by plant density, plant age, depth to groundwater, and accessible soil moisture due to precipitation infiltration. The interaction of plants with groundwater is the primary focus of this research (Schorr et al., 2017, UACE, 2000).

Evapotranspiration (ET) was applied to the model using the EVT package. The ET flux (in units of length per time) is applied to each related model cell in the domain by the EVT Package (Panday et al., 2017). ET is the entire amount of groundwater removed by evaporation and transpiration of plants is referred to as evapotranspiration. Several factors can influence ET, which include the depth of water table, soil texture, vegetation, plant density, root depth, and plant types etc. Increased root density and depth improve evapotranspiration. Coniferous forests deplete groundwater more than deciduous woods (Shi et al, 2020). In this study, EVT rate used were ranged 12.5 - 25 inch per year (Figure 17). Furthermore, mesquite rooting depths can reach up to 30 feet, where the majority of plant roots were shallow, ranging from 6 to 20 feet, with intricate root systems that may transfer water to deeper roots (rather than extract from them)

during particular time periods (Scanlon et al, 2005). An extinction depth of 30 ft was used by Chowdhury and Mace (2017) but this resulted to an inland depression (Panday et al., 2017). So in this model, 10 ft of extinction was applied, which was taken from the calibrated EVT values from TWDB Transport Model (Panday et al., 2017). Live Oak woodlands in Brooks and Kenedy counties, crop lands in Hidalgo and Cameron counties, and mesquite scrub lands near the Rio Grande all have quite high real ET rates. In Hidalgo, Jim Hogg, and Willacy counties, regions with relatively low actual ET rates often correlate with metropolitan areas and bare crop land (Schorr et al., 2017).

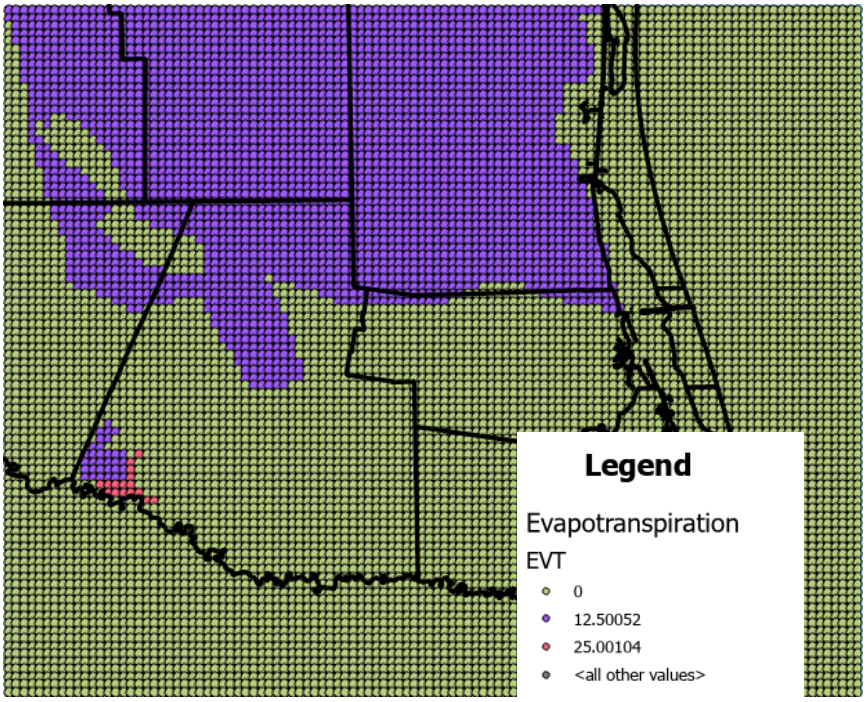

Figure 17. Distribution of EVT in the model domain. The distribution is taken from the Transport model 2017. The colored cells are all 12.5 inch/yr except for the red cells which are 25 inch per year green cells are 12 inch/yr, while blue cells are 12 inch/yr and light green cells are 12 inch/yr.

Parameter calibration

The model was calibrated using an automatic calibration utilizing Parameter Estimation (PEST), an industry-standard inverse modeling software tool developed by Watermark Numerical Computing (2004) (Hutchison et al., 2011; Doherty, 2010). PEST was originally created to speed up the process of model calibration, in which values for model parameters are reverse calculated by comparing model outputs to system state data. A model's "parameters" can represent the qualities of the materials in which processes simulated by the model occur, the stresses that originate and maintain those processes, or both. Pest differed from previous parameter estimating software by operating in a model-independent manner; it communicates with a model via the model's own input and output files (Doherty, 2018). During calibration, the hydraulic conductivity values were changed to produce the best fit between observed and simulated groundwater levels. To calibrate the model, manual modifications and automatic calibration with PEST were used. As it was mentioned earlier to calibrate the model, Chicot and Evangeline aquifers were used as the targets, which will have greatest number of wells (treated as control points in the model).

The mathematical foundations of the PEST nonlinear parameter estimation algorithm are shown below. Function of *M* represents the relationship between parameters and model-generated observations. Function *M* maps n-dimensional parameter space into *m*-dimensional observation space. Assume that the matching set of parameters consist of the vector b_0 is the corresponding set of model-calculated observations (generated using M) is c_0

$$c_0 = M(b_0) \tag{1.3}$$

Taylor's theorem tells us that the following relationship is approximately correct for generating a collection of observations c corresponding to a parameter vector b that differs very slightly from bo, with the approximation improving with proximity of b to b_0:

$$c = c_0 + J(b - b_0)$$

(1.4)

Where J is M's Jacobian matrix, i.e., the matrix with m rows (one for each observation), and the n elements of each row being the derivatives of one observation with respect to each of the n parameters.

To create a set of model parameters for which the model-generated observations are as near to set of experimental observations as possible in terms of least square sense, ie., to determine a parameter set for which the objective function (φ) (equation 1.5), is minimum.

$$\varphi = (c - c_0 - J(b - b_0))^t Q\ (c - c_0 - J(b - b_0))$$

(1.5)

Where Q is the diagonal matrix/weight matrix and c in equation 1.5 now represents the experimental observation vector. Replacing $(b - b_0)$ with u as parameter upgrade vector on the basis of the vector $(c - c_0)$ which defines the difference between the model-calculated observations c_0 and their experimental counterparts c. The equation becomes: (Doherty, 2010)

$$u = (J^t Q J)^{-1} J^t Q (c - c_0)$$

(1.6)

MAR scenarios

According to Paup et al., (2021), Hidalgo, Cameron and Willacy alone have a projected cumulative amount of 886,255 acre-ft ($3.86x10^{10}$ ft^3) per year of water needs (potential shortages) in year of 2020. This research aims to understand how much water that can be injected without flooding the are and to recover this injected water to alleviate the shortages. A four injection wells, spaced about ¼ miles away from each other will be modeled near existing and recommended desalination plants from 2016 region M plan (Figure 22). Four scenarios compose of 1-year continuous injection and 5-year continuous injection will both be carried out in Layer 1 and Layer 2. Layer 1 and Layer 2 are considered as permeable zones i.e., decent sand content. Additionally, assigning K values are needed to be observed since a high k value would move the injected water from the capture area (Lowry and Anderson, 2006). The areas selected are near a FEMA flooding area where water can be up to 5 ft deep during a flood event (Figure 23). To assess the capabilities of MAR applications in the region; this study uses different injection rates at different depths and injection period. For 1 year continues injection, the water will be injected from 12/31/2014 to 12/31/2015, and for 5-year continues injection, the water will be injected from 12/31/2013 to 12/31/2018. Changes in water level will be observed for every injection rates. This study will also analyze how each of the different rates affect the water budget system. Lastly, this research will observe the system in response to different hydraulic conductivity values. Figure 18 shows a well on Layer 1 and the well screen can't be seen in this picture, while Figure 19 shows that the well screen is open below Layer 1 (Layer 2)

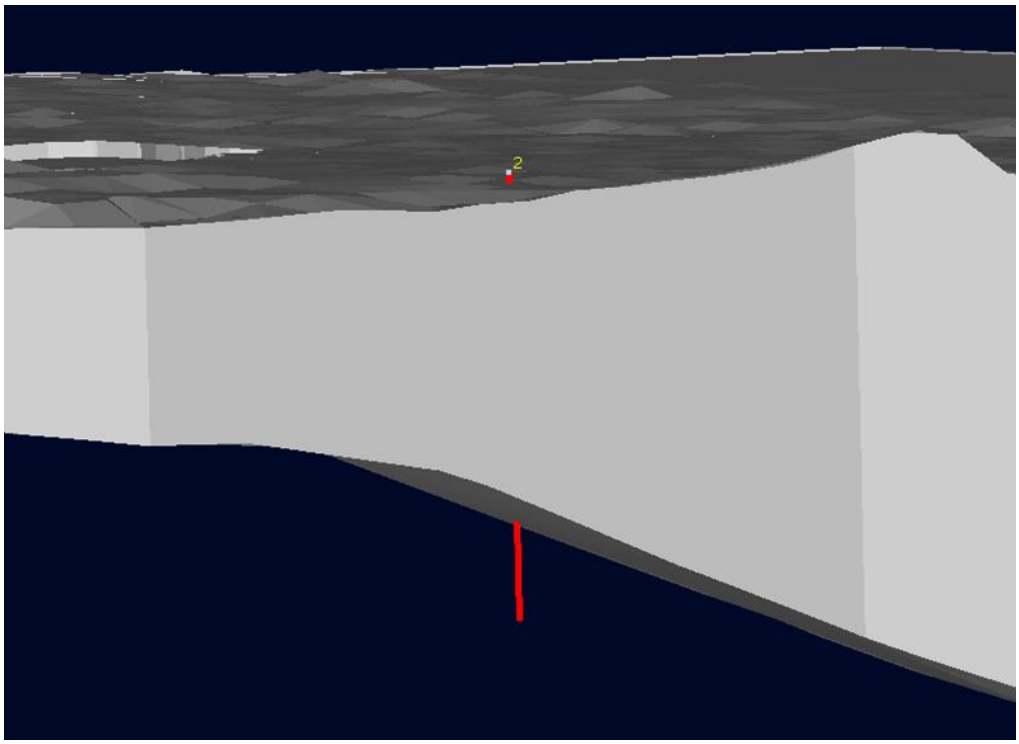

Figure 18. Well in Layer 1. The screen is open in -150 to -200 ft below sea level

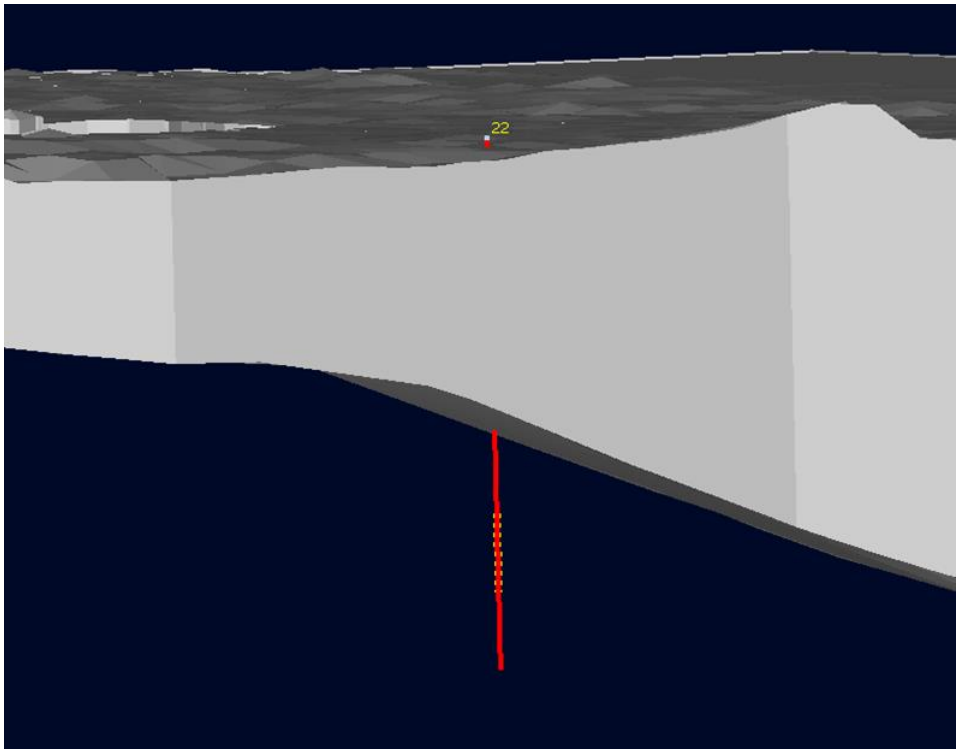

Figure 19. Well screen open in Layer 2. The screen is open in -350 to -400 ft below sea level

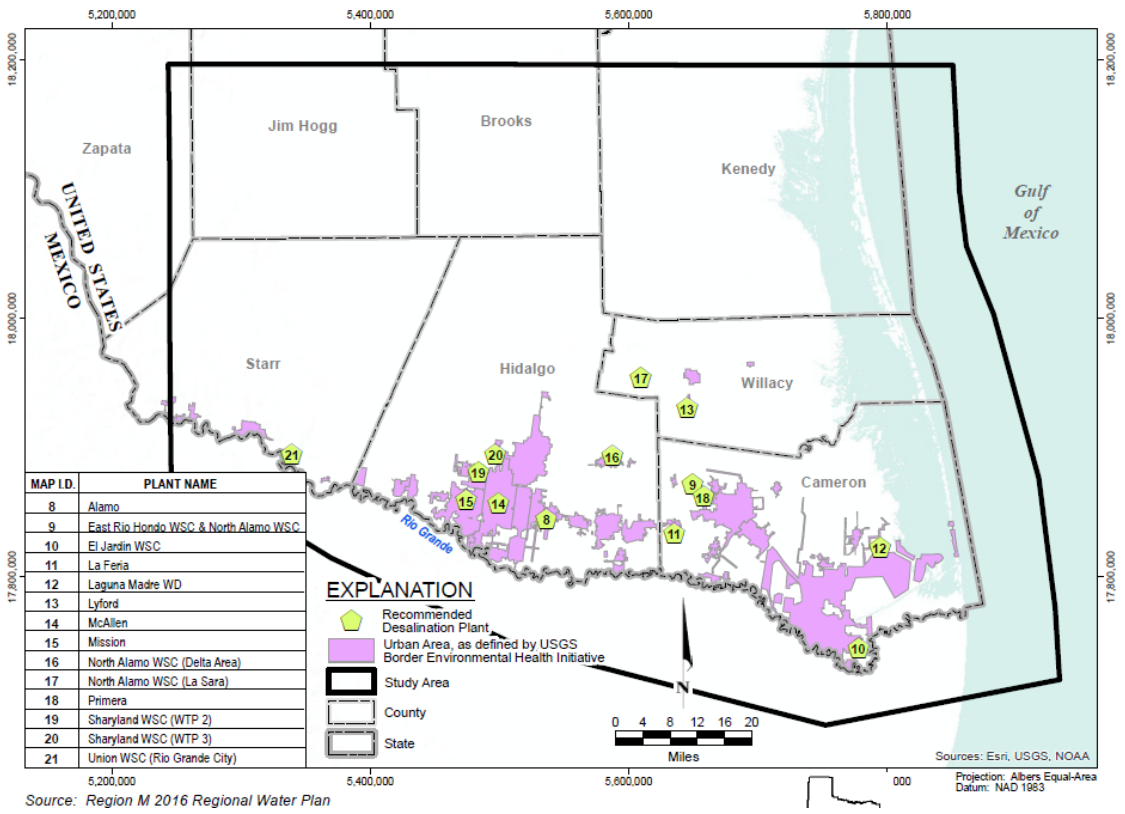

Source: Region M 2016 Regional Water Plan

Figure 20. Recommended brackish groundwater desalination plants in Lower Rio Grande Valley

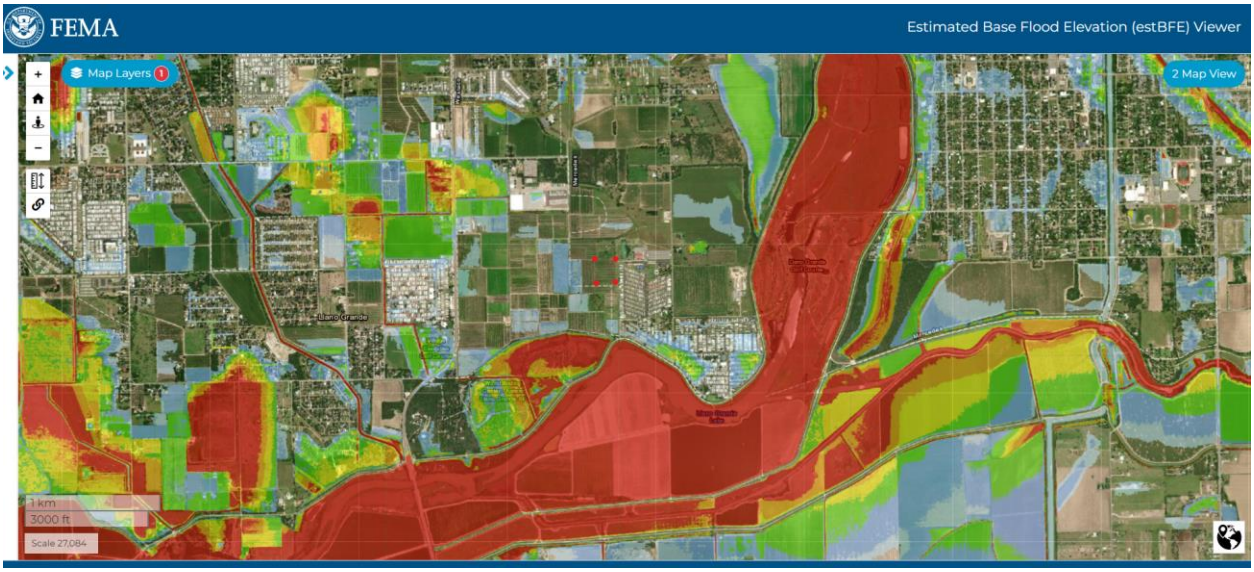

Figure 21. MAR location and estimated water depths above land surface during 1% annual storm event. Red depicts flood water 5 ft and greater (FEMA, 2022).

The base scenario was created by assuming recharge from the calibrated model's steady state condition (Stress Period 1) and pumping are held constant from 2013. (Stress Period 30). All other time-based package used the parameters from the steady state. Projected target volume and injection rate for every target layer are shown in Table 9.

Table 9. Model scenario and target volume. Volumes in ft^3

Injection Rate (cfd) per well (4 well)	**Target volume of water injected in 12/31/14 – 12/31/15 Layer 1**	**Total Volumetric Budget 12/31/14 – 12/31/15 Layer 2**	**Total Volumetric at the end of injection 12/31/13 – 12/31/18 Layer 1**	**Total Volumetric at the end of injection 12/31/13 – 12/31/18 Layer 2**
500	7.30E+05	7.30E+05	3.65E+06	3.65E+06
1000	1.46E+06	1.46E+06	7.31E+06	7.31E+06
10000	1.46E+07	1.46E+07	7.31E+07	7.31E+07
100000	1.46E+08	1.46E+08	7.31E+08	7.31E+08
250000	3.65E+08	3.65E+08	1.83E+09	1.83E+09
500000	7.30E+08	7.30E+08	3.65E+09	3.65E+09

CHAPTER IV

RESULTS AND DISCUSSION

Parameter calibration results

Figure 21 shows the parameter changes for all pilot point groups in every iteration. For most problems, 5 to 6 optimization iterations will be required for model calibration (Doherty, 2010). Table 10 shows the statistics result of the calibration. The calibration result has a residual mean of 1.97 ft. Compared to Panday and others (2017), this study shows a higher absolute residual mean and RMS errors. It is important to note that the 2017 model incorporated more layers and had a larger model area. Observation data points were included in the 2017 report. The Coefficient of determination (R^2) in this study is 0.93 (Figure 23). Figure 23 shows the comparison of calibrated heads to observed heads.

The mean head residual displays the residuals' sensitivity to the parameter value, indicating whether the heads have increased or reduced as a result of the parameter change. The RMS head error sensitivity measures how much the difference between observed and modeled water levels has changed (Panday et al., 2017).

RMS error is at 16.1 which is 3% of the hydraulic head drop (highest observed head minus the lowest observed head used in calibration), and is within 10 percent error commonly pursued for model calibration (Chowdhury & Mace, 2007). Model verification is a proof that the calibrated model matches a collection of field data that is independent to the data used to calibrate the model (Ander et al., 2015). Calibrated models were further verified by comparing it

to other water levels observed in different years. We used observation water levels from the Chicot (Model layer 1-3) and Evangeline (Model Layer 3-6) from 1984-85, 1998-99 and 2011-13 (figure 24-28.). This observation well groups were taken from the 2017 LRGV Transport geodatabase by Panday and colleagues. The figure shows wells located in the Chicot aquifer and some are in the Evangeline Aquifer. Some wells have screens open on multiple aquifers ,yet the Visual MODFLOW determine the location of the well according to assigned observation point level. Since some wells are drilled in multiple wells.

Table 10. Calibration statistics

	This Model (Number of Targets: 75)	**TWDB 2017 Transport Model (Number of Targets: 81)**
Maximum Residual (ft)	32.07	39.69
Minimum Residual (ft)	-73.35	-33.82
Residual Mean	2.1	0.29
RMS Error	16.1	11.82
RMS Error %	3%	< 4%
Coefficient of determination	0.93	0.97

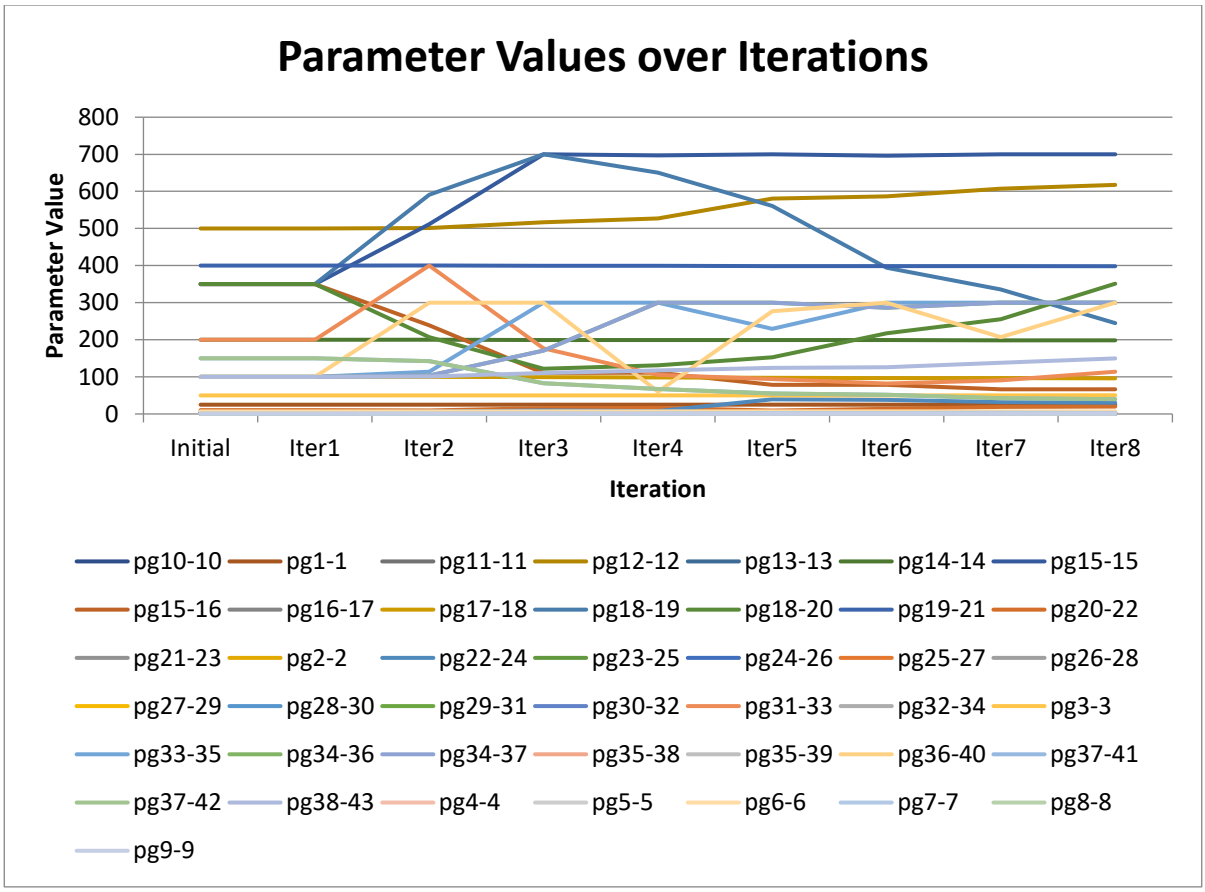

Figure 22. Parameter changes throughout the iterations.

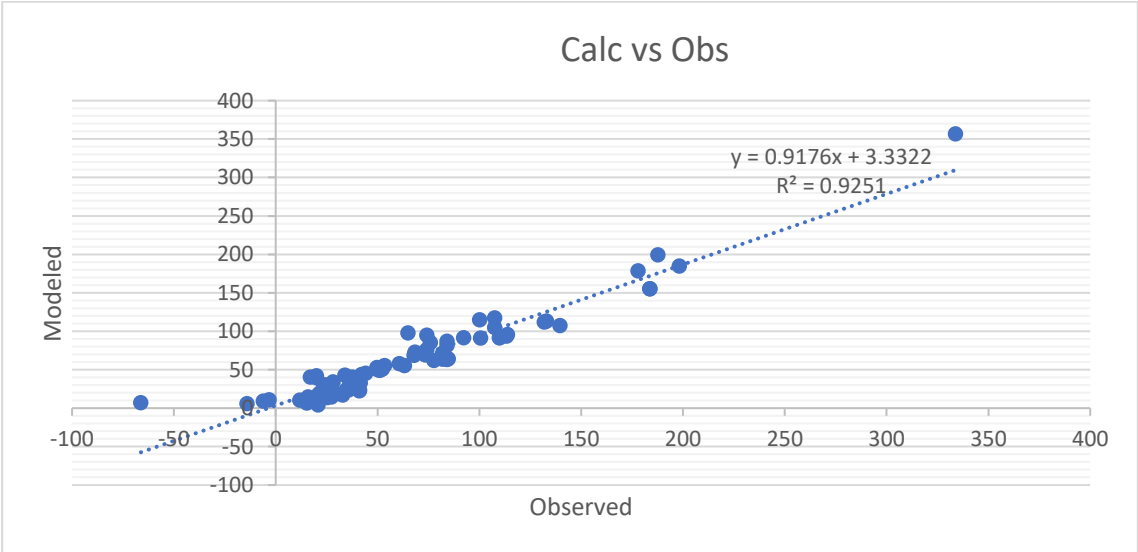

Figure 23. Calculated heads vs Observed heads

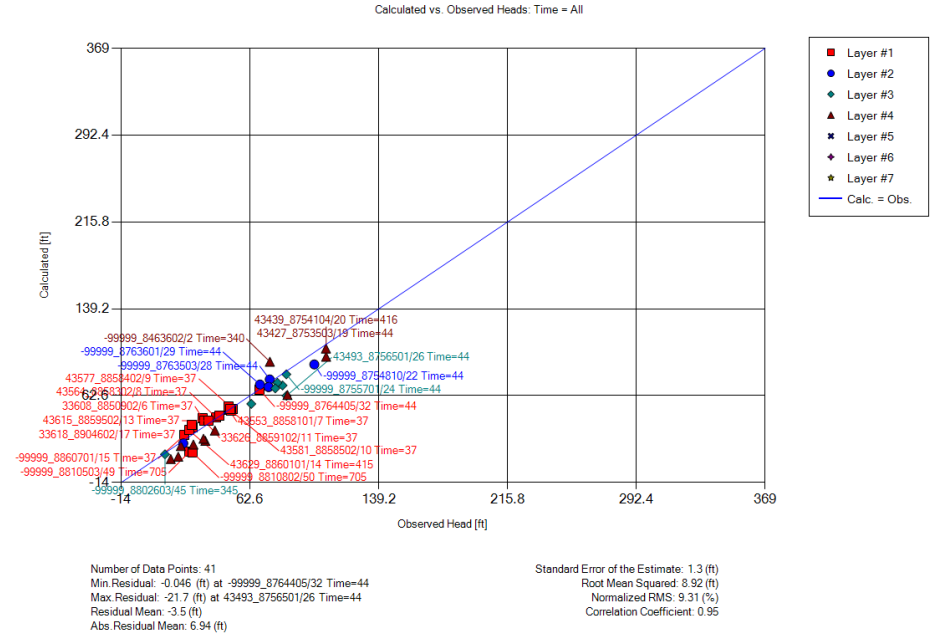

Figure 24. Chicot (1984 – 1985) Calculated vs observed heads.

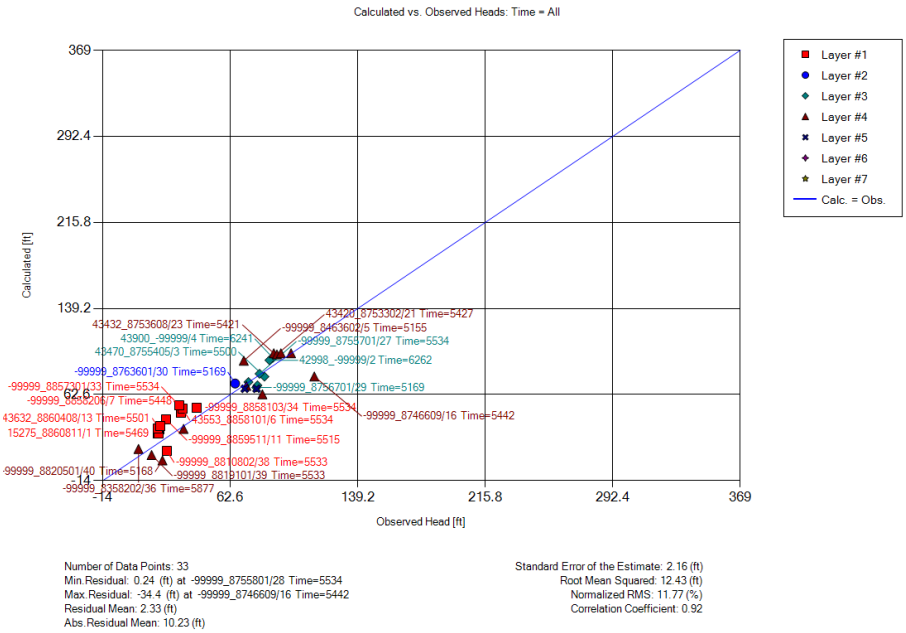

Figure 25. Chicot (1988 – 2001) Calculated vs observed Heads.

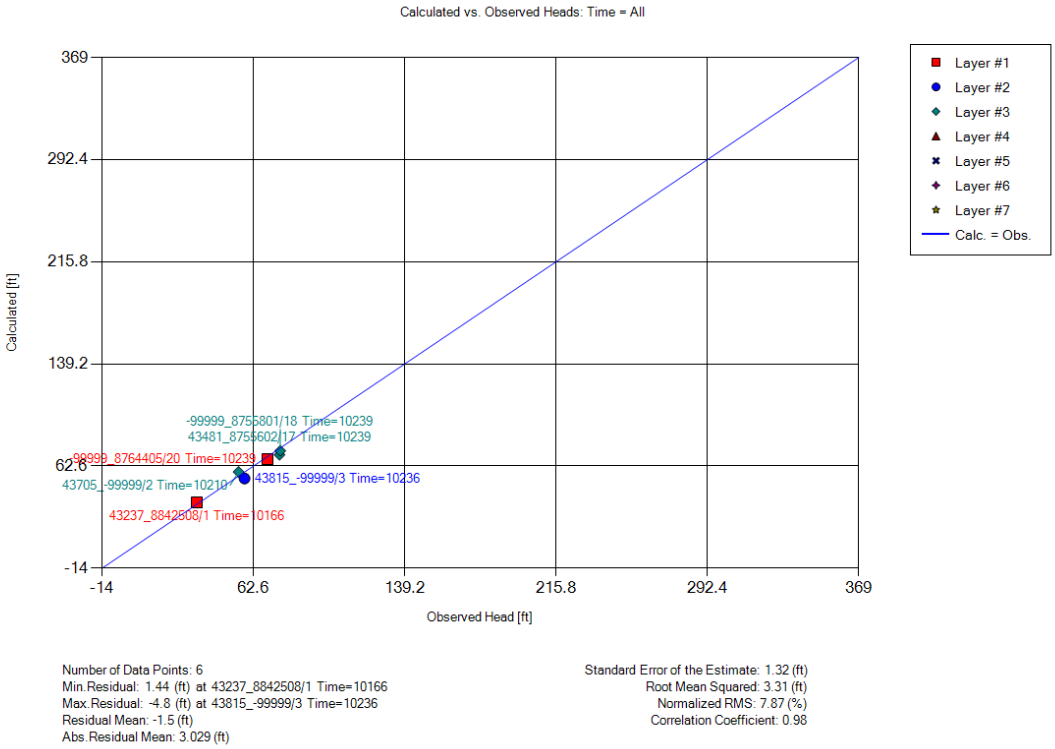

Figure 26. Chicot (2011 – 2012) Calculated vs observed Heads.

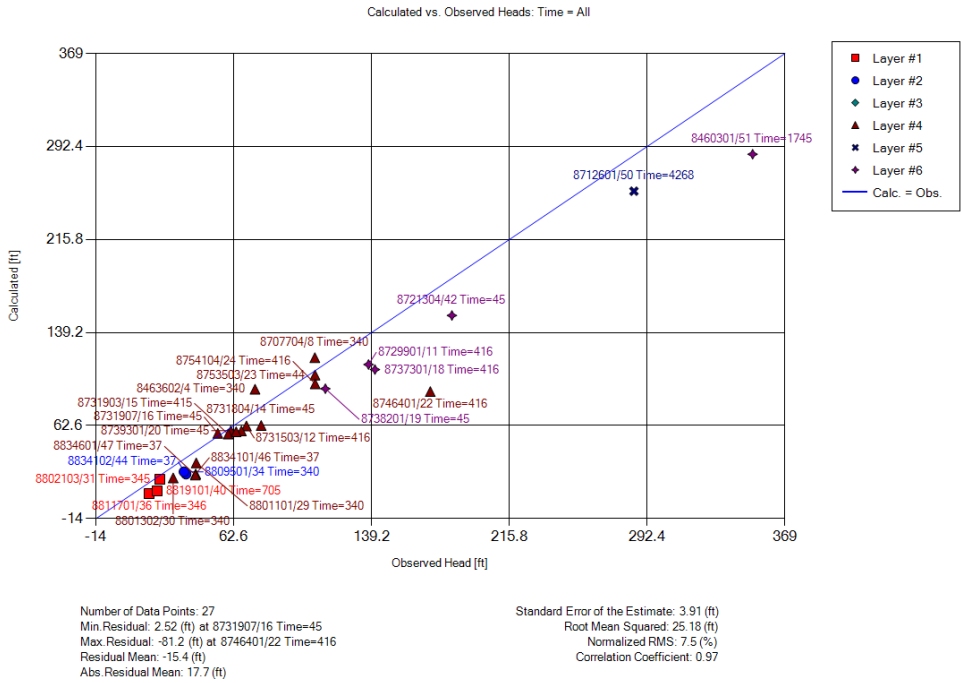

Figure 27. Evangeline (1984-1988) Calculated vs observed Heads.

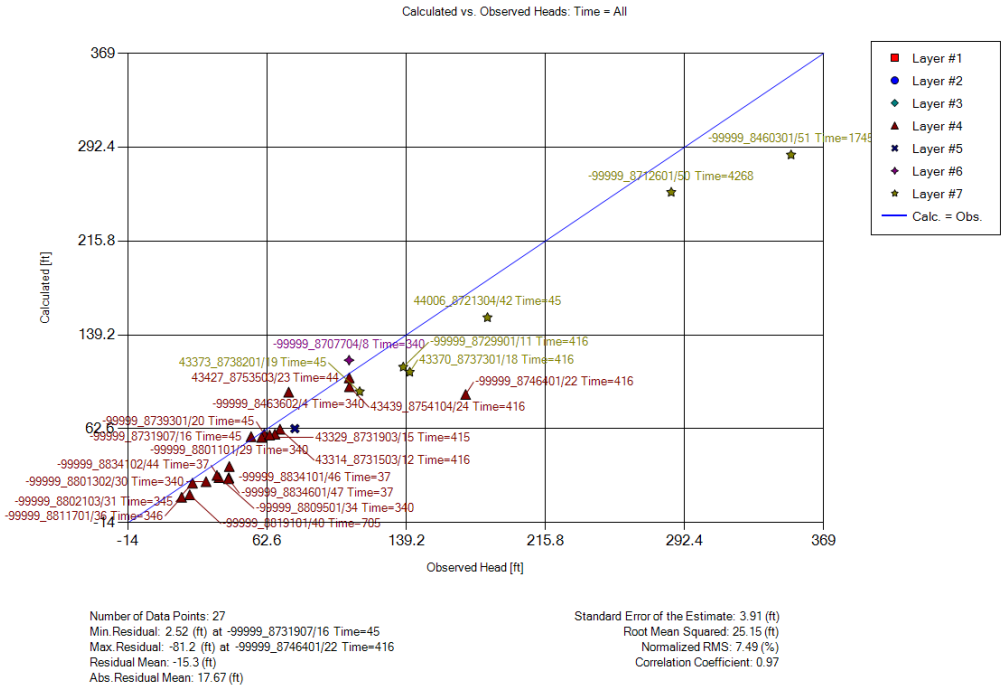

Figure 28. Evangeline (2011 – 2012) Calculated vs observed Heads.

Sensitivity analysis

The Jacobian matrix is calculated for the majority of PEST iteration. The model must be run at least m times during this process, where m is the number of configurable parameters. PEST writes composite parameter sensitivities to a "parameter sensitivity file" called case.sen immediately after calculating the Jacobian matrix, where case is the current case name (i.e., the filename base of the current PEST control file) (Doherty, 2018).

PEST records the sensitivity of each parameter to the observation dataset as it calculates derivatives to a file that is constantly available for review. If it is determined that the behavior of specific parameters (usually the least sensitive ones) is impeding PEST's performance during the optimization process, these parameters can be temporarily retained at their existing values while

PEST calculates a suitable upgrade for the remaining parameters (Doherty, 2010). Figure 16 shows the sensitivity of all the hydraulic conductivities in the model. Table 11 shows the sensitivity analysis at last iteration. PEST searches for parameter upgrades after each iteration, and it is possible that some parameters are sensitive during the initial iterations when their values are close to their starting values but become insensitive at the end of the inversion process, corresponding to a more calibrated status. As a result, sensitivities often fluctuate during the inversion process. Insensitive parameters generally mean it has no effect on the calibration for observations.

Table 11. Sensitivity analysis of last iteration. "pg" means the pilot point group to which the parameter belongs to.

Parameter	**Iter8**	**Parameter**	**Iter8**
pg10-10	0.276622	pg24-26	0.000787
pg1-1	0.148549	pg25-27	0.00703
pg11-11	1.60079	pg26-28	3.84E-05
pg12-12	0.006532	pg27-29	1.45E-05
pg13-13	0	pg28-30	0.000352
pg14-14	0.359052	pg29-31	0.00032
pg15-15	0.105531	pg30-32	0.007045
pg15-16	0.10494	pg31-33	2.42E-05
pg16-17	0.053197	pg32-34	0
pg17-18	0.067335	pg3-3	0.220323
pg18-19	0.106227	pg33-35	9.49E-05
pg18-20	0.106229	pg34-36	9.66E-05
pg19-21	0.325579	pg34-37	9.66E-05
pg20-22	0.000764	pg35-38	0.00191
pg21-23	0.003657	pg35-39	0.00191
pg2-2	0.478832	pg36-40	1.45E-06
pg22-24	0.000966	pg37-41	0.000539
pg23-25	0.007962	pg37-42	0.000539
pg6-6	1.65708	pg38-43	0.000596
pg7-7	0.000208	pg4-4	0.076978
pg8-8	0.002189	pg5-5	0.003161
pg9-9	0.043904		

Observed water level

Table 12 shows the total water volume injected compares to the projected amount of water to be injected. A total of 28 simulations were done to simulate the proposed scenarios. Figure 29 and 30 shows the water elevation Above Mean Sea Level (amsl) of the injection area in 1- and 5-year year injection, respectively. In general, Layer 1 produced higher water elevation mounding during injection. Lower injection rates from 500 cfd to 10000 cfd, did not show any clear mounding of the water table. The results show that 500,000 cfd injection that the water level rose to 59 ft which is about 4 ft below the top of the cell (ground surface). All simulated injection rates were not able to flood the cell where the water is being injected. However, some of the surrounding cells that has a lower surface elevation that is likely to be a river, or a lake and had a closer water elevation. The water table is still below the surface of the cell which means that this lower depression area is still not flooded.

Table 12. Total expected amount and actual injected volume

Injection rate per well	Expected amount in 1 year	Expected amount in 5 years	Total Volume Amount Injected in 1 year	Total Volume Amount Injected in 5 years	Total Volume Amount Injected in 1 year in Layer 2	Total Volume Amount Injected in 5 years in Layer 2
500	7.30E+05	3.65E+06	7.30E+05	3.65E+06	7.30E+05	3.65E+06
1000	1.46E+06	7.30E+06	1.46E+06	7.30E+06	1.46E+06	7.30E+06
10000	1.46E+07	7.30E+07	1.46E+07	7.30E+07	1.46E+07	7.30E+07
100000	1.46E+08	7.30E+08	1.46E+08	7.30E+08	1.46E+08	7.30E+08
250000	3.65E+08	1.83E+09	3.65E+08	1.83E+09	3.65E+08	1.83E+09
500000	7.30E+08	3.65E+09	7.30E+08	3.65E+09	7.30E+08	3.65E+09

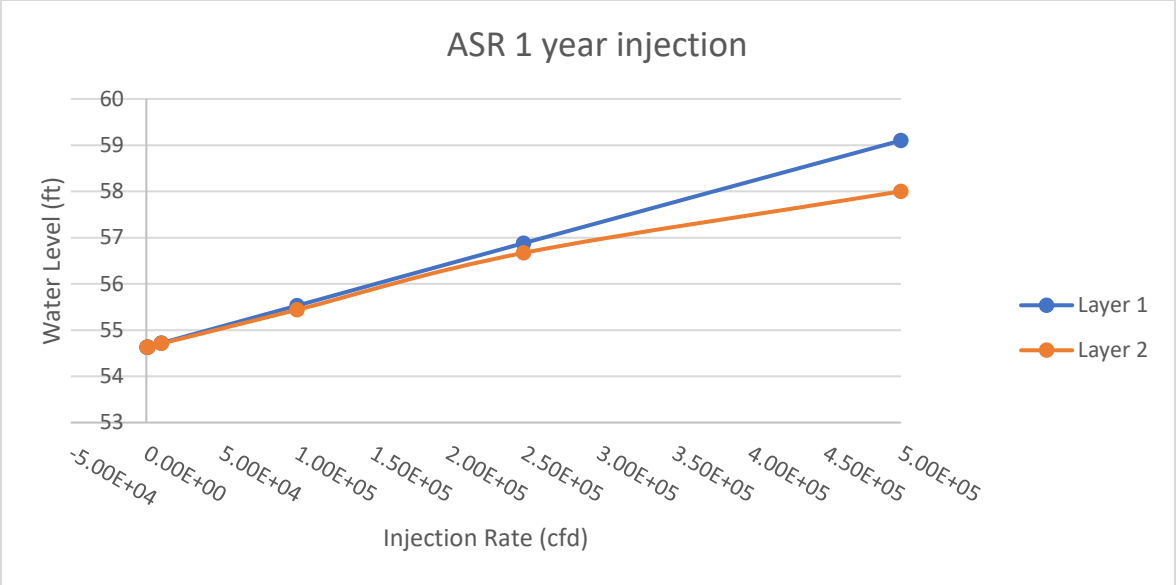

Figure 29. Water elevation (amsl) at the MAR site at the end of 1 year injection period. Top of the cell is at 63 ft asml

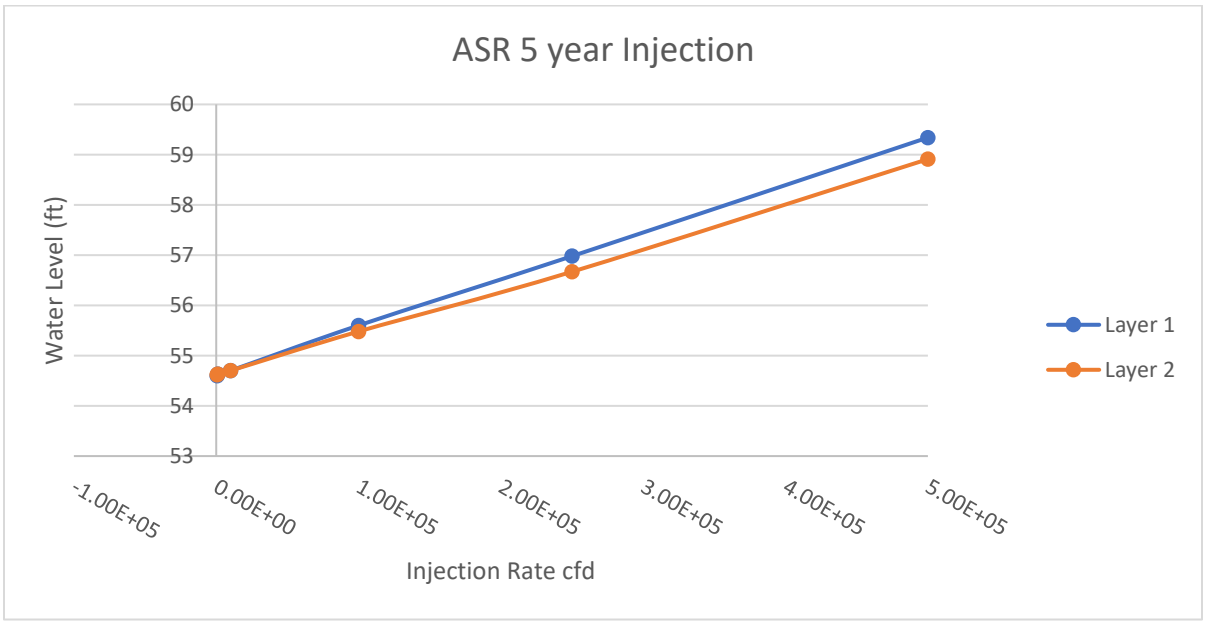

Figure 30.Water elevation (amsl) at the MAR site at the end of the 5-year injection period . Top of the cell is at 63 ft asml

Figure 31 through 34 shows the observed the water level changes through time. Figure 54 – 57 summarize each injection period. This observation also shows that obvious increase of water level in the MAR area is only visible by injecting 100,000 cfd per well of higher. For 1-

year continuous injection, the water level went down after a year of no injection. The peak water level for each injection rate is consistent for 5 years of injection base scenario. Appendix A shows individually the water changes for each scenario and injection rates.

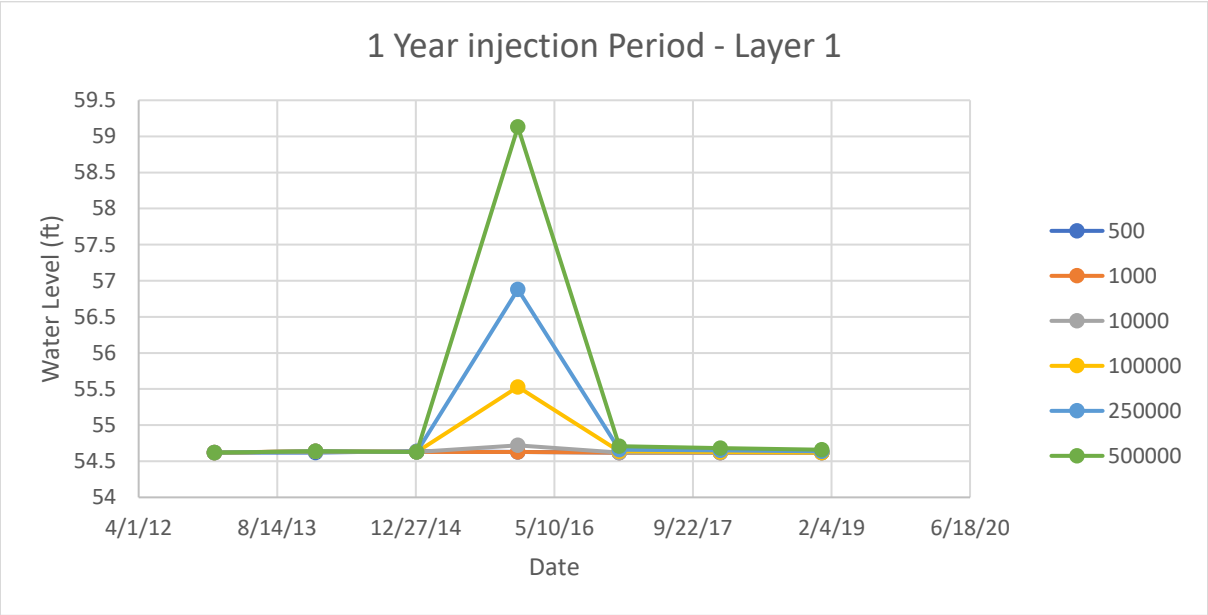

Figure 31. Summary of water level for 1 year of injection period in layer 1

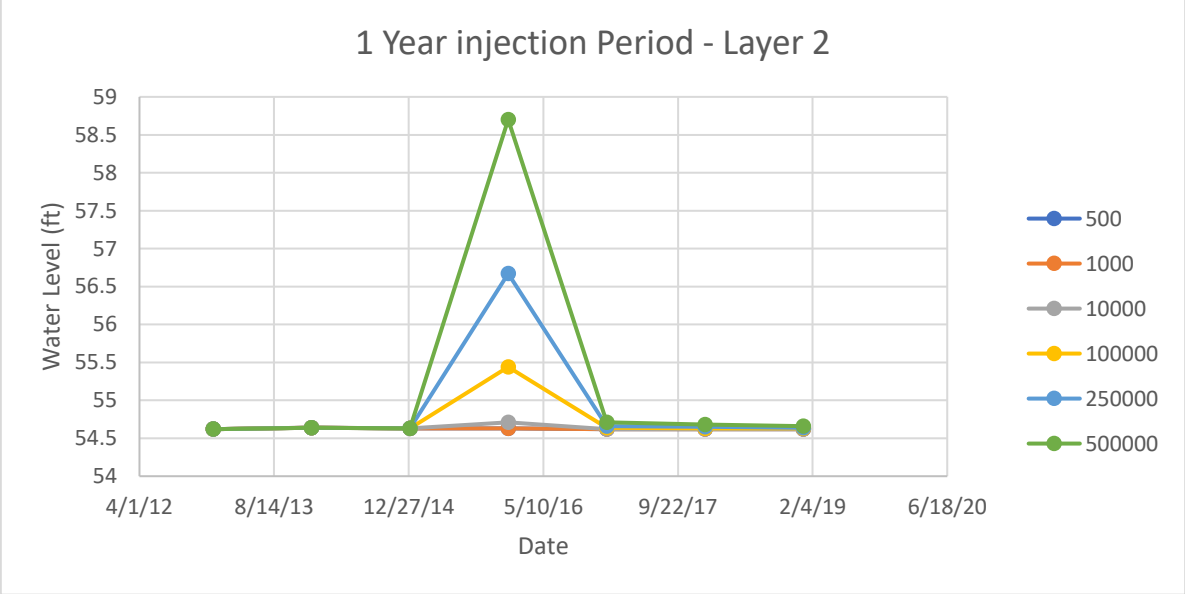

Figure 32. Summary of water level for 1 year of injection period in Layer 2

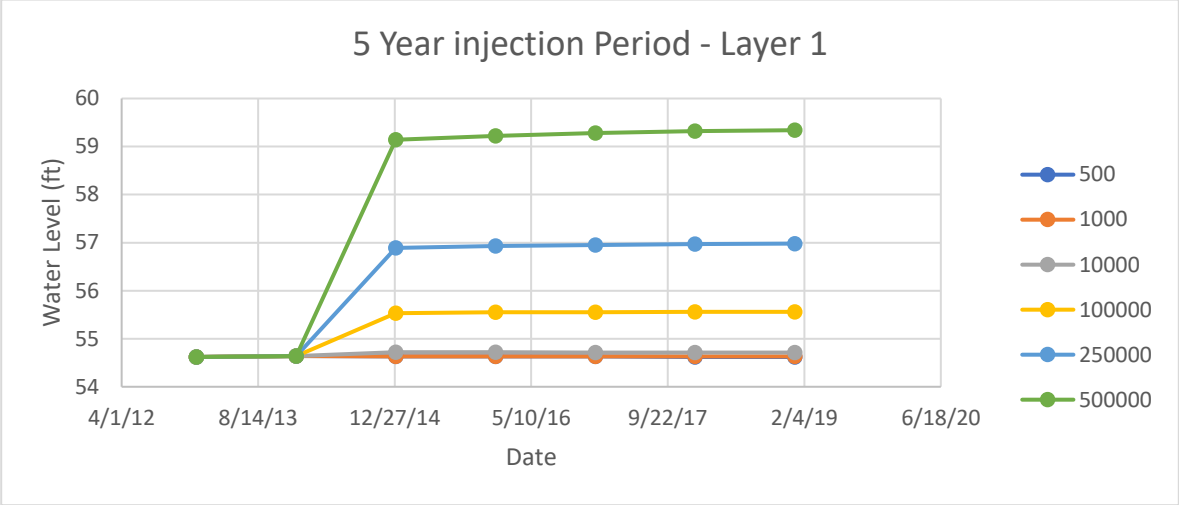

Figure 33. Summary of water level for 5 year of injection period in layer 1

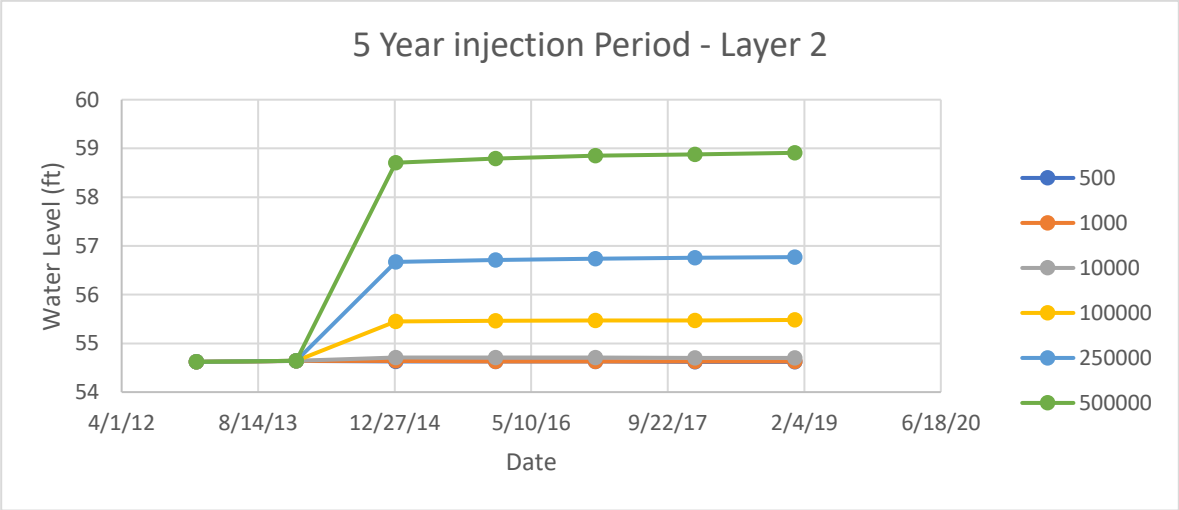

Figure 34. Summary of water level for 5 year of injection period in layer 2

Water budget comparison

To examine the changes in water level, especially on why lower rates did not result to high mounding, this study also looks at the water budget and compare the water entering and leaving the system. When an MAR is applied, there is an increase in the amount of groundwater that is leaving the system through storage, river boundary, ET, and Constant Head. For lower injection rates, the water that leaves the system through Storage outflow and River outflow

increased. Only at higher injection rate that the water that leave the system through Constant Head and ET increased. Figures 35-38 show the comparison of how much water is leaving the system for each boundary. Other boundaries such recharge, GHB, and Well are all equal for the same stress periods and time-steps. It can be observed that ET and Constant Head responded differently compared to other boundaries. The possible explanation is because ET is a function head, it is possible that some cells went below the bottom cell of the top layer therefore, ET was negligible.

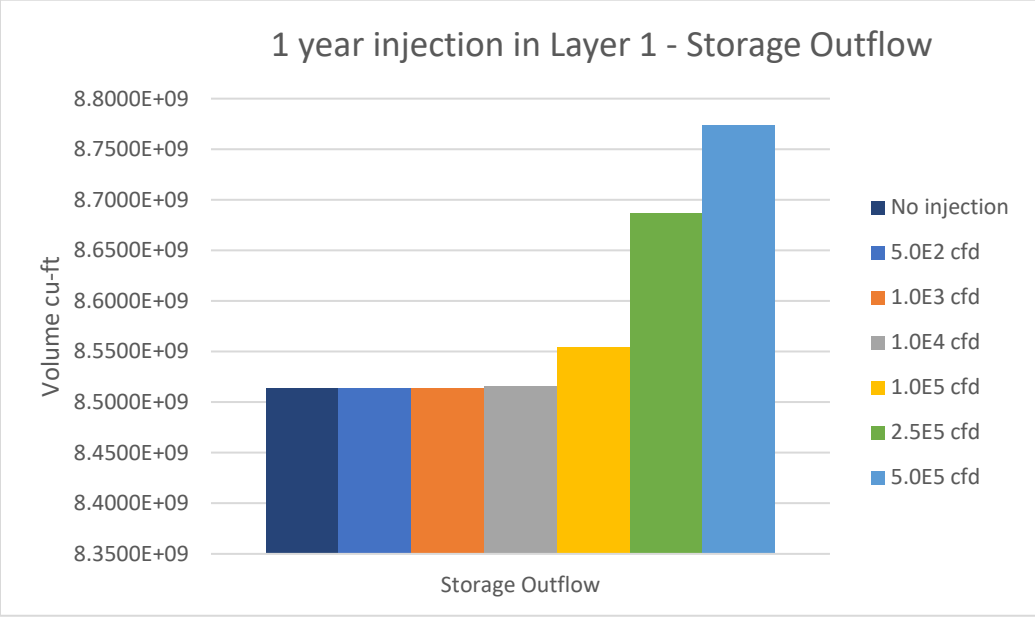

Figure 35. Comparison between the Storage outflow budget of a model without injection and with an MAR application

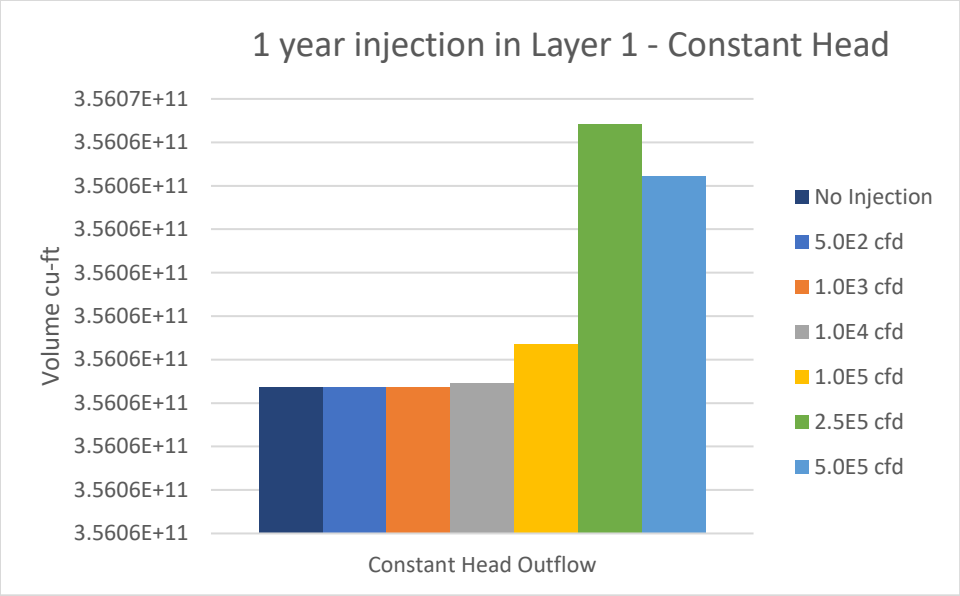

Figure 36. Comparison between the Constant Head outflow budget of a model without injection and with an MAR application

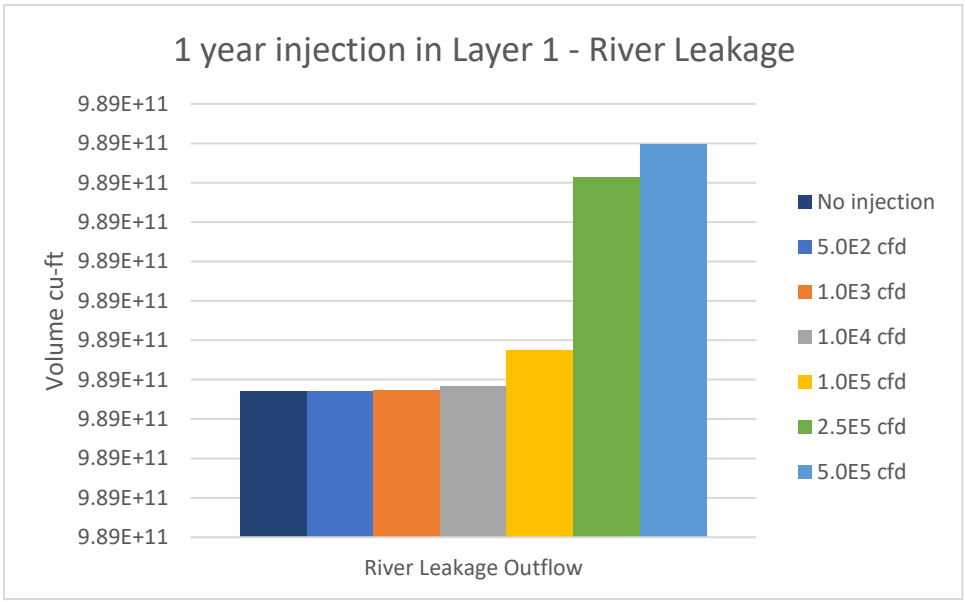

Figure 37. Comparison between the River Leakage outflow budget of a model without injection and with an MAR application

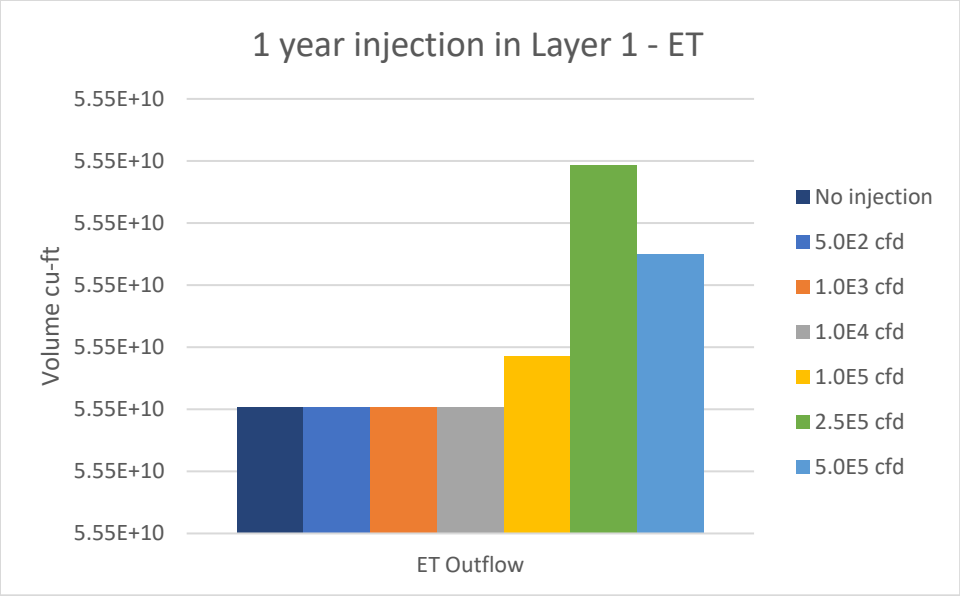

Figure 38. Comparison between the ET outflow budget of a model without injection and with an MAR application

Observation of changes in different hydraulic conductivities

This study also evaluated how the groundwater model and MAR application response to different K values. Using two scenarios (B1 – 10,000 & 100,000 cfd), different multipliers were applied to hydraulic conductivity near the MAR site. Table 13 shows differnt K value that were used to changed the K value of the injection area in model Layer 1 and Model Layer 2. Each variation were applied on 1 layer depending on which layer the injection is being applied. Fewer simulations were done on Layer 2 as it follows the same pattern on Layer 1. Table 14 also shows the changes to the water level by applying different multipliers to the K values of the MAR site. The changes in water level by applying different multiplier is almostt insignificant. Lower K values resulted in slightly higher water level for an injection rate of $1.0x10^5$ ft^3/d.

Table 13. Hydraulic conductivity value of the injection area(layer) in different multiplier (ft/d)

	x.5	x1	x2	x10	x50
Layer 1 (kx)	182.08445	364.1689	728.3378	3641.689	18208.445
Layer 1 (kz)	7.46816	14.93632	29.87264	149.3632	746.816
Layer 2(kx)	201.0773	402.1546	804.3092	4021.546	20107.73
Layer 2 (kz)	122.63115	245.2623	490.5246	2452.623	12263.115

Table 14. Water level changes at different K applied on Layer 1

Injection Rate per well (cfd)	x0.5	x1	x2	x10	x50
1000	54.62 ft	54.63 ft	54.66 ft	54.73 ft	54.75 ft
10000	54.72 ft	54.72 ft	54.72 ft	54.76 ft	54.78 ft
100000	55.76 ft	55.53 ft	55.37 ft	55.19 ft	55.15 ft

Figure 39 to 45 are bar graphs comparing each boundaries showing the amount of groundwater coming in and out of the system. Boundaries that are not included are constant throughout the model: Well In (Injection), GHB, and Recharge boundary. Constant Head in and out both shows a decreasing amount of groundwater as the K values increase. The difference between two scenarios is that a lower injection rate results in a lower CHD outflow volume compared to higher injection rate. For River inflows and outflows, both shows an increasing pattern, but the lower injection rate shows a slightly higher inflow while the higher rate shows a higher outflow volume. ET outflow shows a pattern of increasing outflow of groundwater with increasing K value, although higher injection rate shows a slightly higher outflow. Both injection rate shows that the Storage inflow and outflow shows a pattern of decreasing volume of groundwater with increasing K values. Slower injections rates shows a significant inflow while a faster injection rate shows a higher storage outflow.

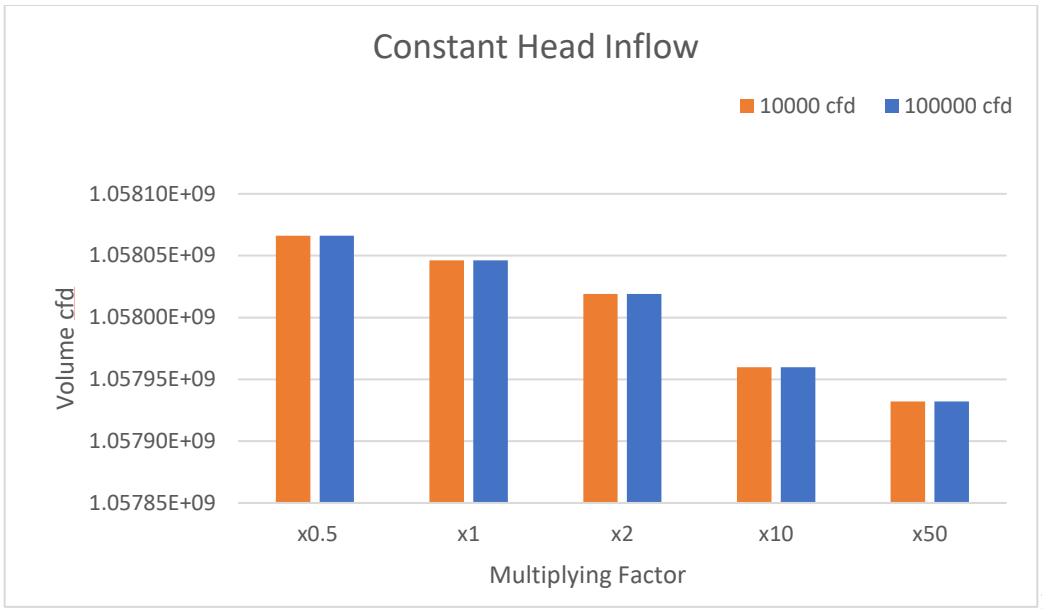

f

Figure 39. Constant Head inflow volume budget of scenario 10,000 cfd and 100,000 cfd with different K values applied in the injection area

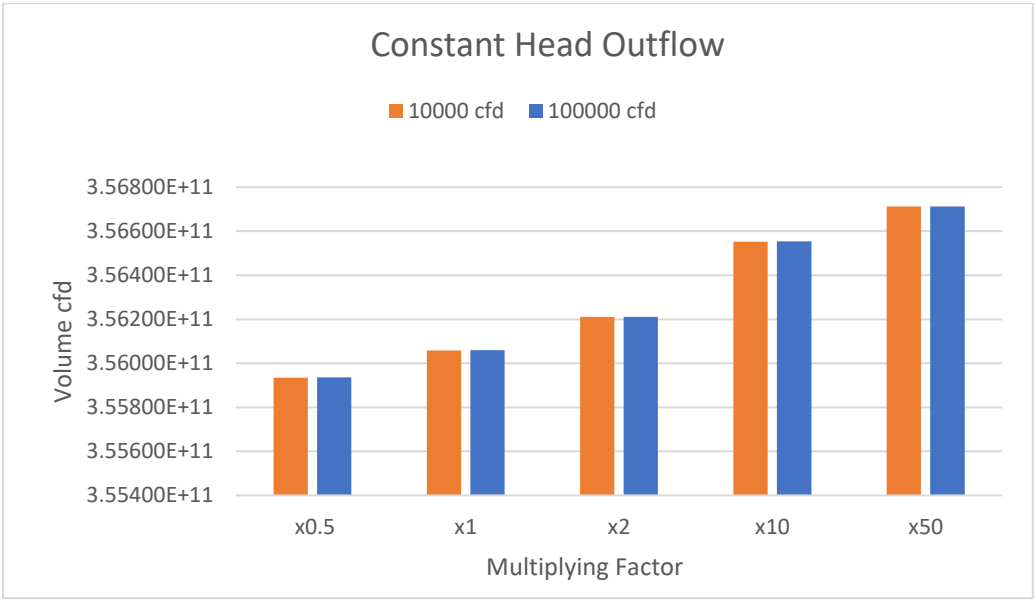

Figure 40. Constant Head outflow volume budget of scenario 10,000 cfd and 100,000 cfd with different K values applied in the injection area

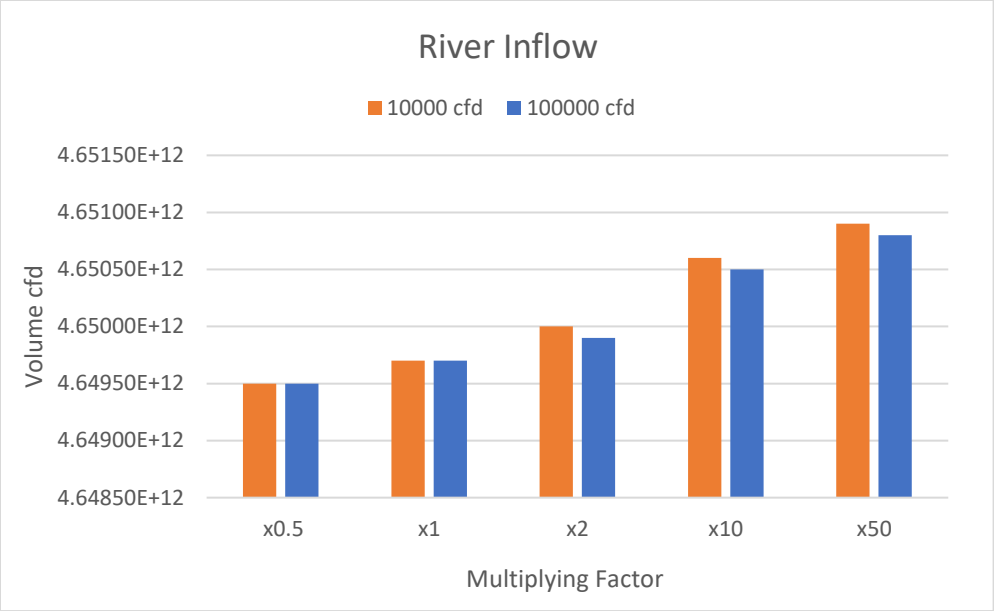

Figure 41. River inflow volume of scenario 10,000 cfd and 100,000 cfd with different K values applied in the injection area

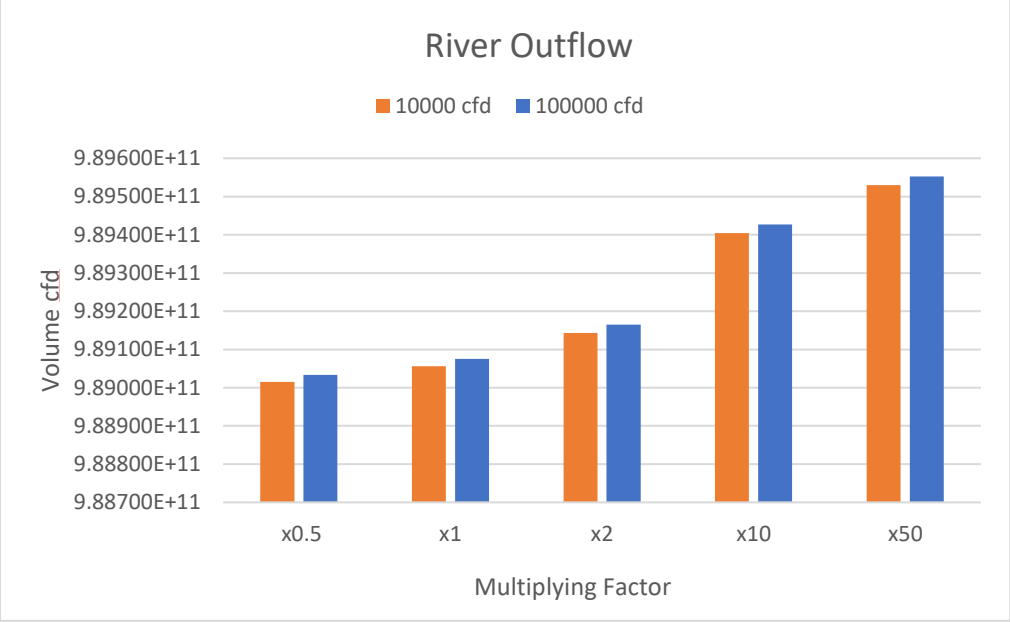

Figure 42. River outflow volume of scenario 10,000 cfd and 100,000 cfd with different K values applied in the injection area

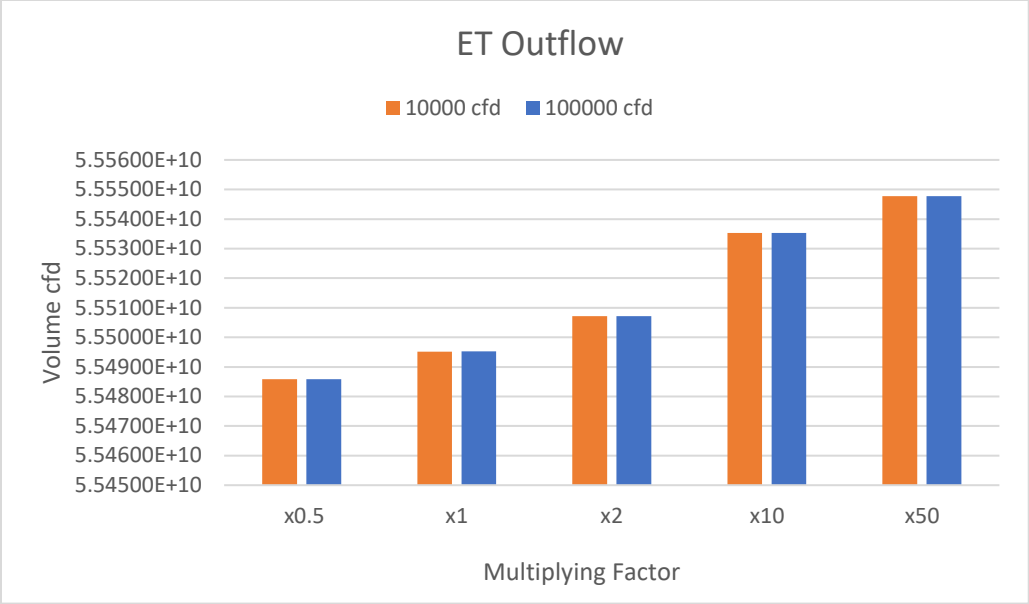

Figure 43. ET volume of scenario 10,000 cfd and 100,000 cfd with different K values applied in the injection area

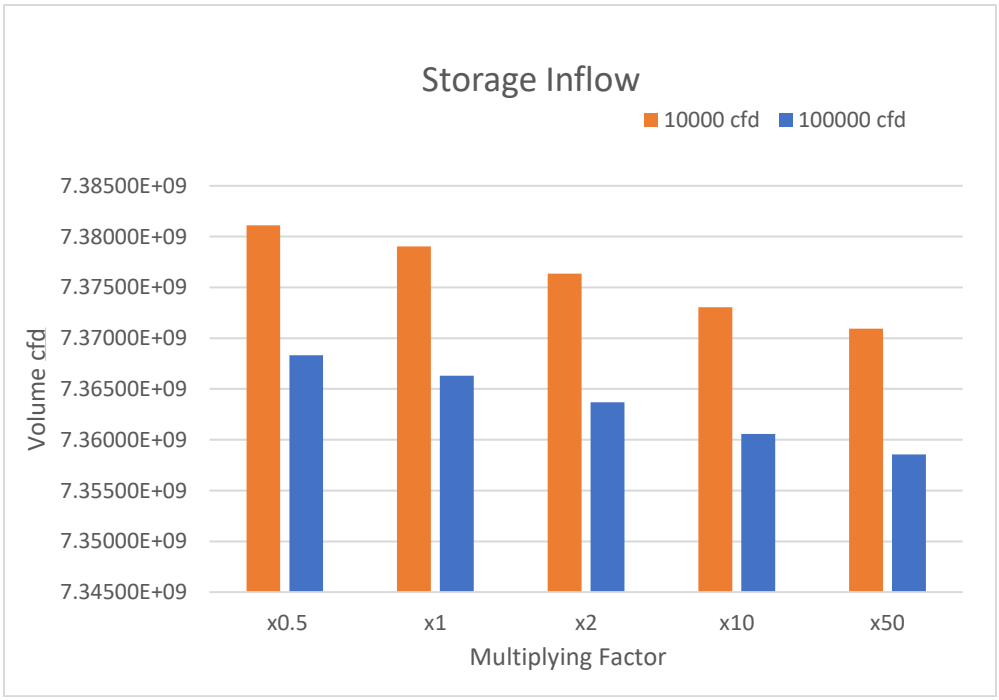

Figure 44. Storage inflow volume of scenario 10,000 cfd and 100,000 cfd with different K values applied in the injection area

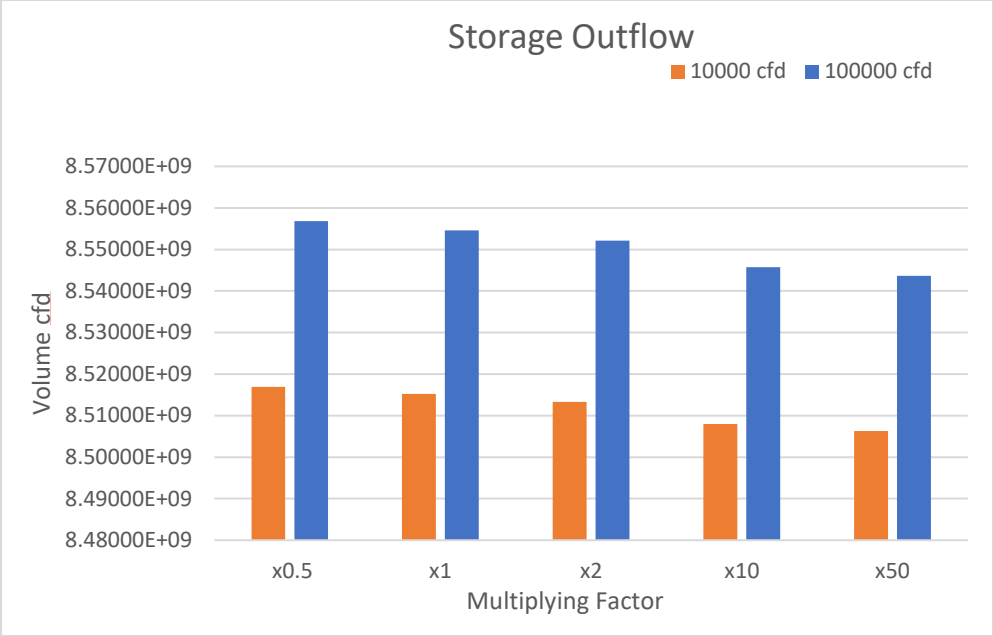

Figure 45. Storage outflow volume of scenario 10,000 cfd and 100,000 cfd with different K values applied in the injection area

MAR examination of performance for flood events

The flow rate during storm events in July of 2020 and June 2018 is reported in Table 15. These flow rates were taken from a river gauge in San Benito during these events. Table 15 also shows the highest cumulative injection rates for 4 wells ($5x10^5$ cfd x 4 wells). By comparing the flow rate of MAR and these flooding events, this study found that cumulative injection rate of this study's MAR is less than 1% of the flow rate during this storm event.

Table 15. Highest cumulative injection rates of MAR and flow rates during storm events

Total Highest Injection rate for four wells in 1 year of injection	**Total Highest Injection rate for four wells in 5 years of injection**	**Flow rate in the river during Hurricane Hanna July 25th - 27th , 2020**	**Heavy rainfall resulted from widespread flooding on June 18th – 22nd of 2018**
$2x10^6$ ft^3/d (15 MGD)	$2x10^6$ ft^3/d (15 MGD)	$3.36x10^8$ to $6.11x10^8$ ft^3/d (2,513 – 4,570 MGD)	$1.32x10^8$ to $2.30x10^8$ ft^3/d (987 – 1,720 MGD)

Model limitations

Like many other models, simulated results can provide useful insight for policy maker and decision making. The information provided from this study should be used with caution as there were limitations when this model was built, e.g., limited data available, simplified boundary conditions etc., which include and not limited to, monitoring data from region; modeling outcomes (boundary conditions); calibrations based on available data/info when building the site conceptual model; scenarios (focusing on aquifer responses to injections/quantity; despite of water quality).

CHAPTER V

CONCLUSION

The goal of this study is to simulate MAR to improve regional water security and potentially mitigate flood hazards. Outcomes of this project identified water quantity and flow rates that can be injected into the targeted hydrogeologic units in LRGV. With a groundwater flow model calibrated with historical data, twenty eight (28) scenarios of simulation of water injections to the aquifer were conducted. At a rate of 100,000 cfd and higher, injection at layer 1 and layer 2 showed an increase in water level in the cells where the injection occurs and as well as adjacent cells. The adjacent cells had a water elevation to ground surface, but this area shown to be a creek or a canal. The flow model also showed how an increase in water injection affected the regional water budget. ET and Constant Head Outflow did not show any increase in outflow volume for slower rates. Increase in ET and Constant Head outflow can only be seen higher $1.0x10^5$ and $5.0x10^5$ ft^3/d. At lower injection rates, there was an increase in water flowing out of the River and Storage outflow. Overall, as the injection rate increased, the outflow for all boundaries also increased. A higher injection rate also resulted in more water leaving the modeling domain through ET and Constant Head. As the K values increased, the amount of groundwater seemed to decrease in both the Constant Head input and outflow volumes. Both the volume of River inflows and outflows exhibited an upward trend. The pattern of the ET outflow indicated that the outflow of groundwater increased when K values increases. Both the inflow

and outflow rates from the storage demonstrated a pattern of declining groundwater volume with increasing K values. Lower injection rates indicated a considerable flow, whereas faster injection rates indicate a greater outflow of stored energy. The change in water level after injection is rather minor. In summary, a higher K values resulted with more flow in the system but did not heavily affect the regional water table.

An amount of 7.30×10^5 to 3.65×10^9 cubic feet of water were able to be injected into the groundwater system without flooding the area (water table not exceeding ground surface). The water injected can be an additional water supply when there is a higher water demand or can be used to alleviate the water demand such as data reported in 2020. Despite the small injection rates (3~5% of flood water from Hurricane Hanna) applied in the simulation compared to the volume in major storm events, MAR can still reduce the stresses brought by these extreme flood events. The number of injection sites and pumping wells can be adjusted as needed to better mitigate of flood hazards that can potentially cause devastating damages to properties and businesses.

Future work

Although study results of MAR show promising results as an alternative mean for improving water security and mitigate flood hazard, it is imperative that more research is needed. For example, assessment of impacts of increasing number of sites/wells at desired locations with adequate K/geological formations with different injection durations. Another important aspect

for MAR would be to consider water quality/geochemical processes and factors such as effectiveness of water recovery.

REFERENCES

1. TWDB. 2012 State Water Plan | Texas Water Development Board. (2012). https://www.twdb.texas.gov/waterplanning/swp/2012/index.asp
2. Bruun, B., Jackson, K., Lake, P., & Walker, J. (2016). Texas Aquifers Study.
3. Chowdhury, A., & Mace, R. E. (2007). Groundwater Resource Evaluation and Availability Model of the Gulf Coast Aquifer in the Lower Rio Grande Valley of Texas (No. 368). Texas Water Development Board. https://www.twdb.texas.gov/publications/reports/numbered_reports/doc/R368/R368_GulfCoastGAM.pdf
4. Gibson, M., Campana, M., & Nazy, D. (2018). Estimating Aquifer Storage and Recovery (ASR) Regional and Local Suitability: A Case Study in Washington State, USA. Hydrology, 5, 7. https://doi.org/10.3390/hydrology5010007
5. Hutchison, H. (2017). Predictive simulation report: Lower Rio Grande Valley Groundwater Transport Model.
6. Khan, S., Mushtaq, S., Hanjra, M. A., & Schaeffer, J. (2008). Estimating potential costs and gains from an aquifer storage and recovery program in Australia. Agricultural water management, 95(4), 477-488.
7. Kimbler, O. K. (1970). Fluid Model Studies of the Storage of Freshwater in Saline Aquifers. Water Resources Research, 6(5), 1522–1527. https://doi.org/10.1029/WR006i005p01522
8. Shaw, K., Stein, Z., Deeds, N., George, P., Milczarek, M., & Yan, Q. (2020). Statewide survey of aquifer suitability for aquifer storage and recovery projects or aquifer recharge projects [abridged]: Report to the 87th Texas Legislature.
9. Lowry, C. S., & Anderson, M. P. (2006a). An Assessment of Aquifer Storage Recovery Using Ground Water Flow Models. Groundwater, 44(5), 661–667. https://doi.org/10.1111/j.1745-6584.2006.00237.x
10. Maliva, R. G., Guo, W., & Missimer, T. M. (2006). Aquifer Storage and Recovery: Recent Hydrogeological Advances and System Performance. Water Environment Research, 78(13), 2428–2435. JSTOR.
11. Maliva, R., Guo, W., & Missimer, T. (2005). Hydrogeology and aquifer storage and recovery system performance. Gulf Coast Association of Geological Societies, 55, 473–485.
12. M.J. Streetly. (1998). The Use of Modeling to Predict the Behavior of ASR Systems. In Artificial Recharge of Ground Water (1st ed., pp. 263–267). CRC Press.

13. Modeling aquifer storage and recovery potential for seasonal water storage in the Flemish alluvial plains of Belgium using MODFLOW | SpringerLink. (n.d.). Retrieved March 31, 2021, from https://link.springer.com/article/10.1007/s12517-020-5190-6

14. Schorr, S., Hutchison, W. R., Panday, S., & Rumbaugh, J. (2017). Conceptual Model Report: Lower Rio Grande Valley Groundwater Transport model. Texas Water Development Board

15. Pirnie, LLC, M., ASR Systems, LLC, Jackson, Sjoberg, McCarthy & Wilson, LLP, & Texas Water Development Board. (2011). An Assessment of Aquifer Storage and Recovery in Texas (#0904830940). Texas Water Development Board. https://www.twdb.texas.gov/publications/reports/contracted_reports/doc/0904830940_AquiferStorage.pdf .

16. Pyne, R. D. G. (1995). Groundwater Recharge and Wells, a guide to Aquifer Storage and Recovery.

17. 2021 Rio Grande Regional Planning Group Planning Group Water Planning Group. (2020b). 2021 Rio Grande Water Plan Group.

18. Sallam, O. (2019). Use of Numerical Groundwater Modeling to Assess the Feasibility of Aquifer Storage and Recovery (ASR) in the Wadi Watir Delta, Sinai, Egypt. Journal of Water Resource and Protection, 11, 1462–1480. https://doi.org/10.4236/jwarp.2019.1112085

19. Shi, J., Boghici, R., & Anaya, R. (2020). Draft Conceptual Model Report: Gulf Coast Aquifer System in Groundwater Management Areas 15 and 16. Austin, TX: Texas Water Development Board

20. Smith, W. B., Miller, G. R., & Sheng, Z. (2017). Assessing aquifer storage and recovery feasibility in the Gulf Coastal Plains of Texas. Journal of Hydrology: Regional Studies, 14, 92–108. https://doi.org/10.1016/j.ejrh.2017.10.007

21. Stuyfzand, P. J., Smidt, E., Zuurbier, K. G., Hartog, N., & Dawoud, M. A. (2017). Observations and Prediction of Recovered Quality of Desalinated Seawater in the Strategic ASR Project in Liwa, Abu Dhabi. Water, 9(3). https://doi.org/10.3390/w9030177

22. TWDB. (2020). Statewide Survey of Aquifer Suitability for Aquifer Storage and Recovery Projects or Aquifer Recharge Projects [Abridged].

23. Vacher, H. L., Hutchings, W. C., & Budd, D. A. (2006). Metaphors and Models: The ASR Bubble in the Floridan Aquifer. Groundwater, 44(2), 144–154. https://doi.org/10.1111/j.1745-6584.2005.00114.x

24. Wasif, M. R., & Hasan, M. M. (2020). Modeling aquifer storage and recovery potential for seasonal water storage in the Flemish alluvial plains of Belgium using MODFLOW. Arabian Journal of Geosciences, 13(5), 234. https://doi.org/10.1007/s12517-020-5190-6

25. Yobbi, D. K. (1996). Simulation of subsurface storage and recovery of treated effluent injected in a saline aquifer, St. Petersburg, Florida (Report No. 95–4271; Water-Resources Investigations Report). USGS Publications Warehouse. https://doi.org/10.3133/wri954271

26. Paup, B., & Jackson, K. (2021). 2022 State Water Plan: Water For Texas.

27. Venkataraman, K., Tummuri, S., Medina, A., & Perry, J. (2016). 21st century drought outlook for major climate divisions of Texas based on CMIP5 multimodel ensemble: Implications for water resource management. Journal of hydrology

28. Ward, J. D., Simmons, C. T., Dillon, P. J., & Pavelic, P. (2009). Integrated assessment of lateral flow, density effects and dispersion in aquifer storage and recovery. Journal of Hydrology, 370(1-4), 83-99.

29. Provost, A.M., Reilly, T.E., Harbaugh, A.W., and Pollock, D.W., 2009, U.S. Geological Survey groundwater modeling software—Making sense of a complex natural resource: U.S. Geological Survey Fact Sheet 2009–3105, 4 p..
Venkataraman, K., Tummuri, S., Medina, A., & Perry, J. (2016). 21st century drought

30. Anderson, M. P., Woessner, W. W., & Hunt, R. J. (2015). Applied groundwater modeling: simulation of flow and advective transport. Academic press.

31. Anderson, M. P., & Woessner, W. W. (1991). Applied Groundwater Modeling: Simulation of Flow and Advective Transport (1st ed.). Academic Press.
32. Baalousha, H. (2009). Fundamentals of groundwater modeling. LF Konig, JL Weiss. Groundwater: Modeling Management and Contamination. pp. 113-130.

33. Harbaugh, A. W. (2005). MODFLOW-2005, the US Geological Survey modular ground-water model: the ground-water flow process (Vol. 6). Reston, VA, USA: US Department of the Interior, US Geological Survey.

34. Fetter, C. W. (2000). Applied Hydrogeology, Fourth Edition (4th ed.). Prentice Hall.

35. LaHaye, O., Habib, E. H., Vahdat-Aboueshagh, H., Tsai, F. T. C., & Borrok, D. (2021). Assessment of Aquifer Storage and Recovery Feasibility Using Numerical Modeling and Geospatial Analysis: Application in Louisiana. JAWRA Journal of the American Water Resources Association, 57(3), 505-526.

36. Matthew Webb. (2015). AQUIFER STORAGE AND RECOVERY IN TEXAS: 2015 (No. 15–04). Texas Water Development Board.

37. Shi, J., Boghici, R., & Anaya, R. (2020, September). Draft Conceptual Model Report: Gulf Coast Aquifer System in Groundwater Management Areas 15 and 16. Texas Water Development Board.

38. Hutchison, W. R., Hill, M., Anaya, R., Hassan, M., Oliver, W., Jigmond, M., Wade, S., & Aschenbach, E. (2011, March). Groundwater Management Area 16 Groundwater Flow Model. Texas Water Development Board.

39. Doherty, J. (2018) PEST, Model-Independent Parameter Estimation—User Manual Part 1: PEST, SENSAN and Global Optimisers. 7th Edition, Watermark Numerical Computing, Brisbane

40. Doherty, J. (2010) PEST, Model-Independent Parameter Estimation—User Manual. 5th Edition, with Slight Additions, Watermark Numerical Computing, Brisbane.

41. Snyder, G. L., Pyne, R. D. G., Morrison, K., & Nixon, K. (2022). San Antonio Water System, Texas Carrizo Aquifer Storage Recovery (Asr) Program. Groundwater.

42. Yang, J., Neal, C., Neal, J., Goodrich, J., Simon, M., & Jun, Y. (2016). Decision Support System for Aquifer Recharge (AR) and Aquifer Storage and Recovery (ASR) Planning, Design, and Evaluation - Principles and Technical Basis (No. 600-R-16–222). U.S. Environmental Protection Agency.

43. Statewide Survey of ASR and AR Suitability (2022). In Texas Water Development Board. https://twdb-wsc.maps.arcgis.com/apps/MapSeries/index.html?appid=75313de26daf4994bcb590fdb8846b80

44. Dillon, P., W. Alley, Y. Zheng, and J. Vanderzalm (2022) Managed Aquifer Recharge: Overview and Governance. IAH Special Publication. https://recharge.iah.org/ ISBN 978-1-3999-2814-4

45. Jakeman, A. J., Barreteau, O., Hunt, R. J., Rinaudo, J. D., & Ross, A. (2016). Integrated groundwater management (p. 762). Springer Nature.

46. Kourakos, G., Dahlke, H. E., & Harter, T. (2019). Increasing groundwater availability and seasonal base flow through agricultural managed aquifer recharge in an irrigated basin. Water Resources Research, 55(9), 7464-7492.

47. Alam, S., Gebremichael, M., Li, R., Dozier, J., & Lettenmaier, D. P. (2020). Can managed aquifer recharge mitigate the groundwater overdraft in California's central valley. Water Resources Research, 56(8), e2020WR027244.

BIOGRAPHICAL SKETCH

Dwight Zedric Q. Capus completed his Bachelor of Science in Geology minor in Geographic Information Technology in Sam Houston State University in 2020. He started his graduate studies at UTRGV in M.S. in Ocean, Coastal, and Earth Sciences and was awarded the Master of Science degree in December 2022. He is also a certified 40 HAZWOPER and a certified Geoscience-in-Training (GIT). His email address is dwightzedricc@gmail.com